This is the accepted manuscript version of the final work appeared in *Water Research* that has gone through peer-reviewed and technical editing. To access the final edited and published work, please see https://doi.org/10.1016/j.watres.2020.116255

Modeling the Transport of Neutral Disinfection Byproducts in Forward Osmosis: Roles of Reverse Salt Flux

Jiale Xu[1], Thien Ngoc Tran[2], Haiqing Lin[2], Ning Dai[1*]

[1]Department of Civil, Structural and Environmental Engineering

University at Buffalo, The State University of New York, Buffalo, NY, 14260

[2]Department of Chemical and Biological Engineering

University at Buffalo, The State University of New York, Buffalo, NY, 14260

*Corresponding author: Post address: 231 Jarvis Hall, Buffalo, NY 14260

Phone: (716) 645-4015; Fax: (716) 645-3667

Email: ningdai@buffalo.edu

Abstract

The rejection of disinfection byproducts (DBPs) is an important consideration for the application of forward osmosis (FO) in wastewater recycling. However, the transport of organic compounds in FO is not well predicted by existing models, partially because these models have not incorporated the effect of reverse salt flux, a phenomenon previously shown to influence the transport of pharmaceutical compounds. In this study, we investigated the effects of reverse salt flux on DBP transport in FO and the corresponding mechanisms. We used a commercial Aquaporin membrane and tested sixteen DBPs relevant to wastewater recycling. Using draw solutions constituted by NaCl, $MgSO_4$, or glucose in a bench-scale FO system, we first confirmed that higher reverse salt flux resulted in lower DBP permeance. By integrating results from the bench-scale FO system and those from diffusion cell tests, we showed that two mechanisms contributed to the hindered DBP transport: the steric hindrance in the active layer caused by the presence of the draw solute and the retarded diffusion of DBPs in the support layer via a "salting-out" effect. Lastly, we developed a modified solution-diffusion model incorporating these two mechanisms by accounting for the free volume occupied by draw solute molecules in the active layer and by introducing the Setschenow constant, respectively. The modified model significantly improved the prediction of permeance for halogenated DBPs, and revealed the relative importance of steric hindrance (dominant for large DBPs) and retarded diffusion (dominant for hydrophobic DBPs). The modified model did not accurately predict the permeance of nitrosamines, attributable to their extremely high hydrophilicity or large size.

Keywords: Forward osmosis; Disinfection byproducts; Reverse salt flux; Steric hindrance; Retarded diffusion; Modified solution-diffusion model.

Graphic Art

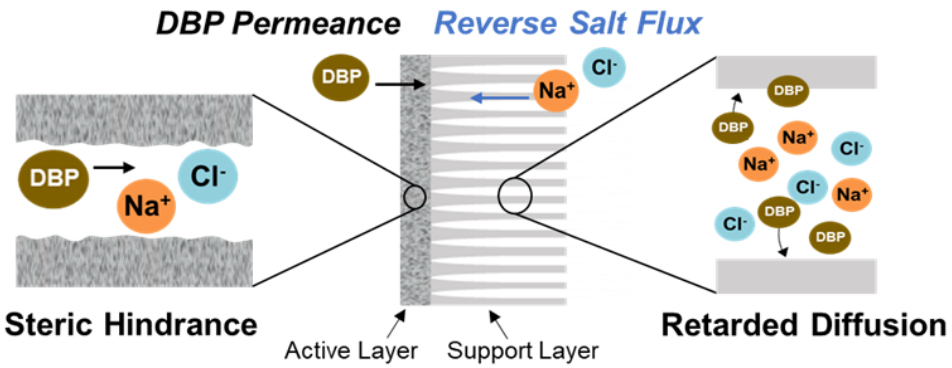
DBP Permeance
Reverse Salt Flux
DBP
Cl-
Na+
Steric Hindrance
Active Layer
Support Layer
Retarded Diffusion

Highlights:

- Reverse salt flux hinders DBP transport through FO membranes.
- Steric hindrance caused by reverse salt flux is stronger on larger DBPs.
- DBP diffusion in the support layer is retarded via a salting-out effect.
- Modified solution-diffusion model improves halogenated DBP permeance prediction.

Nomenclature

A ($m^3 \cdot m^{-2} \cdot s^{-1} \cdot bar^{-1}$)	Water permeance
A_M (m^2)	Contact area of membranes in diffusion cell
$\pi_{D,b}$ (bar)	Osmotic pressure of the bulk draw solution
J_w ($m^3 \cdot m^{-2} \cdot s^{-1}$)	Water flux
J_S ($mol \cdot m^{-2} \cdot s^{-1}$)	Reverse salt flux
J_{DBP} ($\mu g \cdot m^{-2} \cdot s^{-1}$)	DBP flux
$J_{DBP,convection}$ ($\mu g \cdot m^{-2} \cdot s^{-1}$)	DBP flux contributed by convection
R_{DBP} (%)	DBP rejection
B_{FO} ($m \cdot s^{-1}$)	DBP permeance determined in FO experiments
V_F^t (m^3)	Volume of feed solution at time t (s) in diffusion cell
V_D^t (m^3)	Volume of draw solution at time t (s) in diffusion cell
C_F^t ($\mu g \cdot L^{-1}$)	DBP concentration of feed solution at time t (s) in diffusion cell
C_D^t ($\mu g \cdot L^{-1}$)	DBP concentration of draw solution at time t (s) in diffusion cell
C_F^0 ($\mu g \cdot L^{-1}$)	DBP concentration of feed solution at the beginning of the experiments in diffusion cell
C_D^0 ($\mu g \cdot L^{-1}$)	DBP concentration of draw solution at the beginning of the experiments in diffusion cell

C^S (M)	Salt concentration in the support layer
C_z^S (M)	Salt concentration in the support layer at position z
C_i^S (M)	Salt concentration at the interface between the support and active layers (i.e., $z = 0$)
C_D^S (M)	Salt concentration at the interface between the support layer and draw reservoir (i.e., $z = 1$)
$B_{diffusion\ cell}$ ($m \cdot s^{-1}$)	DBP permeance through the entire membrane in diffusion cell
$B_{diffusion\ cell,DI}$ ($m \cdot s^{-1}$)	DBP permeance through the entire membrane in diffusion cell in Milli-Q water
B_{SD} ($m \cdot s^{-1}$)	Modeled DBP permeance through the entire membrane using the conventional solution-diffusion (SD) model
$B_{M\text{-}SD}$ ($m \cdot s^{-1}$)	Modeled DBP permeance through the entire membrane using the modified solution-diffusion (M-SD) model
B_{AL} ($m \cdot s^{-1}$)	DBP permeance through the active layer
B_{AL}^{DI} ($m \cdot s^{-1}$)	DBP permeance through the active layer in the absence of reverse salt flux
B_{AL}^{S}($m \cdot s^{-1}$)	DBP permeance through the active layer in the presence of reverse salt flux
R_r (–)	Retardation factor in the support layer
S (m)	Structure parameter
D_{DBP} ($m^2 \cdot s^{-1}$)	Diffusion coefficient of a DBP in Milli-Q water

D_S ($m^2 \cdot s^{-1}$)	Diffusion coefficient of the draw solute
r_{DBP} (nm)	Molecular radius of a DBP
r_p (nm)	Effective average pore radius in the active layer
r_p^{DI} (nm)	Effective average pore radius in the absence of the salt in the active layer
r_p^S (nm)	Effective average pore radius in the presence of the salt in the active layer
ε (%)	Porosity of the support layer
K_{DBP}^{MSL} (–)	Thickness-averaged partitioning coefficient for a DBP between the support layer and the aqueous solution
$K_{DBP,Salt}^{MSL}$ (–)	Partitioning coefficient for a DBP between the support layer and the saline solution
$K_{DBP,DI}^{MSL}$ (–)	Partitioning coefficient for a DBP between the support layer and Milli-Q water
K_{DI}^{MSL} (–)	Partitioning coefficient for an organic compound between the support layer and Milli-Q water
k_{DBP}^{Salt} (M^{-1})	Setschenow constant of a DBP in saline solutions
$\Delta G_{DBP,j}^{MSL}$ (J)	Free interaction energy between a DBP molecule in the aqueous solution and the membrane support layer
A_{DBP} (m^2)	Contact area between a DBP molecule and the membrane
k ($J \cdot K^{-1}$)	Boltzmann constant (i.e., 1.38×10^{-23} $J \cdot K^{-1}$)

θ (–)	Contact angle
γ_j^{LW} (J·m^{-2})	Apolar surface tension component
γ_j^{+} (J·m^{-2})	Polar electron-accepting surface tension component
γ_j^{-} (J·m^{-2})	Polar electron-donating surface tension component
T (K)	Temperature
MW (g·mol^{-1})	Molecular weight
MV (Å^3)	Molecular volume
ρ (g·L^{-1})	Density
K_{ow} (–)	Octanol/water partitioning coefficient of a DBP or a reference organic compound
ε_{HOMO} (eV)	Energy level of the highest occupied molecular orbital
ε_{LUMO} (eV)	Energy level of the lowest unoccupied molecular orbital
Q^- (a.u.)	Most negative charge on any non-hydrogen atom
Q^+ (a.u.)	Most positive charge on any hydrogen atom

52

1. Introduction

Forward osmosis (FO) is an alternative or supplement membrane technology to reverse osmosis (RO) for wastewater recycling (Linares et al. 2014, Lutchmiah et al. 2014, Qin and He 2014, Yuan et al. 2015, Zou and He 2016). Unlike RO that applies hydraulic pressure to drive water transport, FO utilizes a draw solution with higher osmotic pressure than the feed stream (Lin 2016). Accordingly, FO features lower energy costs (Shaffer et al. 2012, Xiang et al. 2017, Yangali-Quintanilla et al. 2011, Zou et al. 2016) and less irreversible membrane fouling (Jang et al. 2016, Mi and Elimelech 2010, Shaffer et al. 2015) than RO.

Transport of small organic molecules such as disinfection byproducts (DBPs) and pharmaceuticals and personal care products (PPCPs) is an important consideration for wastewater recycling. In FO with sodium chloride (NaCl) or seawater as draw solutions, the transport of PPCPs was slow for large and charged compounds but fast for small and neutral compounds (Alturki et al. 2013, Coday et al. 2014, Xie et al. 2014). DBPs are compounds formed in the reactions between disinfectants and wastewater constituents. Many of the organic DBPs are neutral, halogenated, and/or nitrogenous compounds with lower molecular weight than most PPCPs (Coday et al. 2014, Zeng et al. 2016). DBPs such as trihalomethanes, haloacetonitriles, and *N*-nitrosamines have been detected at 0.01–20 $\mu g \cdot L^{-1}$ levels along the treatment train in full-scale wastewater recycling plants employing RO (Dai et al. 2015, Zeng et al. 2016). The U.S. Environmental Protection Agency (EPA) regulates eleven DBPs for drinking water, including 4 trihalomethanes (EPA 2010), but recent research shows that the unregulated haloacetonitriles and nitrosamines exhibit much higher toxicity than the regulated trihalomethanes and haloacetic acids (Wagner and Plewa 2017), and account for the majority of cytotxicity after integrating the concentration and toxicity of different DBP classes (Lau et al. 2020, Zeng et al. 2016). For potable

reuse, DBPs can pose greater risks to human health than PPCPs (NRC 2012). Our previous study showed that FO can exhibit slightly better rejection than RO for four groups of DBPs (trihalomethanes, haloacetonitriles, haloketones, and nitrosamines) (Xu et al. 2018).

Reverse salt flux, the diffusion of draw solute molecules through the FO membrane to the feed solution (Ferby et al. 2020, Zou et al. 2019, Zheng et al. 2019), has been shown to hinder the forward transport of PPCPs through cellulose triacetate and Aquaporin membranes (Alturki et al. 2013, Kim et al. 2012, Xie et al. 2018, Xie et al. 2012). This phenomenon was attributed to the steric hindrance introduced by the draw solute molecules (e.g., NaCl) present in the membrane matrix, considering that the hydrated radii of sodium and chloride ions were comparable to the radii of the PPCPs investigated as well as the membrane pore radius (Xie et al. 2012). However, a recent study (Sauchelli et al. 2018) using diffusion cells (i.e., without salt gradient across the membrane) found that the permeance of three neutral PPCPs was not affected by the amount of salt present in the membrane. Consistent with the latter, Kim et al. did not observe the hindered forward transport for three relatively hydrophilic PPCPs (Log K_{ow} < 2.6) (Kim et al. 2017). These conflicting results suggest that there are additional mechanisms contributing to the hindered forward transport of organic molecules in FO. The difference observed for PPCPs with different degrees of hydrophobicity suggests that the partition of organic compounds into the organic polymeric membrane may have affected the transport process (i.e., retarded diffusion). Moreover, unlike that in RO, the membrane support layer in FO interfaces with solutions of high salinity (i.e., the draw solution); the presence of salt is known to promote the sorption of hydrophobic organic compounds, i.e., the "salting-out" effect (Burant et al. 2017, Ni and Yalkowsky 2003). The salting-out effect has been reported for polysulfone (Cheong et al. 2013), a common material for the support layer of FO membranes (Han et al. 2012, Luo et al. 2018, Qi et al. 2016). A recent study

(D'Haese 2020) also proposed that the sorption of feed organic solutes can play an important role in affecting their transport.

To date, most solute transport models for FO are built upon models originally developed for nanofiltration (NF) and RO (Heo et al. 2013, Jin et al. 2011, Kong et al. 2018, Kong et al. 2014, Kong et al. 2015, Madsen et al. 2015, Xie et al. 2018, Xie et al. 2012, 2014, Xu et al. 2018). These models have not been able to accurately predict the forward transport of organic compounds, presumably because the effects of reverse salt flux have not been incorporated. For example, a pore hindrance model overestimated the rejection of hydrophobic organic compounds (Log K_{ow} > 3.2 at pH 8) whereas underestimated the rejection of small compounds (MW < 180 $g \cdot mol^{-1}$) (Xie et al. 2018). Similarly, the solution-diffusion model exhibited good prediction for the charged haloacetic acids (Kong et al. 2014) and pharmaceuticals (Kong et al. 2015), but poorly predicted the transport of the neutral molecules chloroform and bromoform (Xu et al. 2018) as well as boron (Kim et al. 2012).

The goal of this study is to explore the mechanisms behind the hindered forward transport of organic compounds by the reverse salt flux in FO, with a specific focus on DBPs due to their importance in wastewater recycling. A total of sixteen neutral DBPs were selected as model compounds, including four trihalomethanes, three haloacetonitriles, two haloketones, and seven nitrosamines. DBP permeance was first measured in a bench-scale FO setup with a commercial Aquaporin membrane and different draw solutions, and then in a diffusion cell without cross-membrane salt gradient. Correlations between the change in DBP permeance due to the reverse salt flux and the molecular size or hydrophobicity of DBPs were assessed to show the relative importance of steric hindrance and sorption effects on DBP transport. Lastly, the conventional

121 solution-diffusion model was modified to incorporate the effects of steric hindrance and sorption–
122 induced retarded diffusion to predict DBP transport.

123 **2. Materials and Methods**

124 **2.1. Chemicals and Membranes**

125 EPA 521 nitrosamine mix (2000 $\mu g \cdot mL^{-1}$ of each nitrosamine in methylene chloride), EPA
126 501/601 trihalomethanes calibration mix (2000 $\mu g \cdot mL^{-1}$ of each trihalomethanes in methanol),
127 EPA 551B halogenated volatiles mix (2000 $\mu g \cdot mL^{-1}$ of each DBP in acetone), *tert*-butyl methyl
128 ether (MtBE, > 99.8%), *N*-nitrosodimethylamine-d6 (d6-NDMA, ≥ 98%), polysulfone beads (M_n
129 ~ 22,000), and 1,2-dibromopropane (97%) were purchased from Sigma-Aldrich. Methylene
130 chloride (DCM, ≥ 99.9%), acetonitrile (HPLC grade, 99.9%), sodium chloride (≥ 99.0%), and
131 glycerol (≥ 99.5%) were purchased from Fisher Chemical. Sodium sulfate (≥ 99.0%) was obtained
132 from Macron. Dichloroacetonitrile (DCAN, > 98%), glucose (99%), magnesium sulfate ($MgSO_4$, >
133 99.5%), and diiodomethane (99%) were obtained from Alfa Aesar. *N*-nitrosodimethylamine
134 (NDMA, 99.5%) was purchased from Chem Service. All chemicals were used as received. DBP
135 substocks (5 $mg \cdot L^{-1}$) were prepared in acetonitrile. All aqueous solutions were prepared using
136 Milli-Q water.

137 A commercial FO membrane, Aquaporin membrane (A/S, Lyngby, Denmark), was used
138 in this study. Aquaporin membrane is a thin-film composite membrane with aquaporin protein
139 embedded in the polyamide active layer. It exhibits higher water permeability and lower reverse
140 salt flux than the conventional cellulose triacetate membrane for FO (Xu et al. 2018). The
141 performance of this membrane in rejecting organic molecules has been tested for PPCPs
142 (Engelhardt et al. 2018, Madsen et al. 2015, Xie et al. 2018) and DBPs (Xu et al. 2018). A previous
143 study has reported that the transport of organic contaminants was dominantly through the

polyamide matrix rather than the aquaporin protein (Xie et al. 2018). The characteristics of the Aquaporin membrane are shown in Table S1. The water flux of the flat-sheet Aquaporin membrane used in this study is consistent with that previously reported for the same membrane (Madsen et al. 2015, Xia et al. 2017).

2.2. Bench-Scale Forward Osmosis Experiments

A bench-scale cross-flow system (Figure S1) was used. It is comprised of a modified permeation cell (SEPA CF II, Sterlitech Corporation) with countercurrent flow for the feed and draw solutions, pressure valves, flow meters, feed and draw solution reservoirs, and two gear pumps (Cole Parmer), as previously described (Xu et al. 2018). The permeation cell holds a membrane with an effective area of 140 cm^2 and features 2 mm channel height on each side. The active and support layers face feed and draw reservoirs, respectively.

Aquaporin membranes were immersed in Milli-Q water for 24 h before the experiments. The draw and feed reservoirs initially contained 2.0 L of draw solution and 1.5 L Milli-Q water, respectively. The draw solutions tested were 1.0 M $MgSO_4$, 1.5 M glucose, 0.5 M NaCl, 1 M NaCl, and 0.2 M NaCl. Crossflow velocity was set at 0.048 $m \cdot s^{-1}$. After a constant water flux was reached (approximately 15 min), DBPs were spiked into the feed reservoir to make up an initial concentration of 20 $\mu g \cdot L^{-1}$ for each halogenated DBP or 10 $\mu g \cdot L^{-1}$ for each nitrosamine. The feed and draw reservoirs were sampled periodically (every 1–2 h) by 5 mL and 15 mL, respectively, for DBP analysis. The molecular properties of all DBPs tested in this study are shown in Table S2. The volume of feed and draw solutions was recorded continuously based on the weight of the reservoirs. Feed solutions were monitored for the change in conductivity (when NaCl or $MgSO_4$ was used as the draw solute) or total organic carbon concentration (when glucose was used as the draw solute) for the calculation of reverse salt flux. Further details on the calculation of water flux,

DBP rejection, DBP permeance, and reverse salt flux are described in Text S1. The external concentration polarization factor of each DBP in the feed solution was considered when calculating DBP permeance. The values of concentration polarization factor are shown in Table S3.

2.3. Diffusion Cell Experiments

A diffusion cell was used to determine DBP permeance in the absence of the reverse salt flux. A membrane coupon (contact area 0.79 cm^2) was sandwiched between two silicone gaskets. The chambers facing the active layer (hereafter referred to as the "feed reservoir") and support layer ("draw reservoir") of the membranes contained 40 mL of the same solution (Milli-Q water, 0.5 M NaCl, or 1.0 M NaCl; i.e., there was no salt gradient across the membrane). Both feed and draw reservoirs were continuously mixed by magnetic stirring at a rate of 200 rpm, to minimize concentration polarization. DBP transport was driven by the DBP concentration difference in the two chambers, with initial concentrations 2 $mg \cdot L^{-1}$ and 50 $\mu g \cdot L^{-1}$ in the feed and draw reservoirs, respectively. Aquaporin membrane coupons were pre-soaked for 24 h in the same solution as that used in the subsequent diffusion test. Over the course of 20 h of the diffusion test, 0.6 mL and 0.1 mL samples were periodically withdrawn from the draw and feed reservoirs, respectively, for DBP analysis. The volume of the samples withdrawn for DBP analysis was accounted for during data processing. The DBP permeance was calculated by:

$$\frac{V_{\mathrm{F}}^{t} \cdot V_{\mathrm{D}}^{t}}{A_M \cdot (V_{\mathrm{F}}^{t} + V_{\mathrm{D}}^{t})} \mathrm{Ln}\left(\frac{C_F^0 - C_D^0}{C_F^t - C_D^t} \right) = B_{diffusion\ cell} \cdot t \qquad (1)$$

where $B_{diffusion\ cell}$ ($m \cdot s^{-1}$) is the DBP permeance through the membrane in diffusion cell; A_M (m^2) is the contact membrane area; V_F^t (m^3) and V_D^t (m^3) are the volume of feed and draw solutions at time t (s), respectively; C_F^t ($\mu g \cdot L^{-1}$) and C_D^t ($\mu g \cdot L^{-1}$) are the DBP concentration of feed and draw solutions at time t, respectively; and C_F^0 ($\mu g \cdot L^{-1}$) and C_D^0 ($\mu g \cdot L^{-1}$) are the DBP concentration of

feed and draw solutions at the beginning of the experiments, respectively. The DBP permeance ($B_{diffusion\ cell}$) was determined using linear regression of equation 1 as a function of t. Duplicate experiments were conducted. The results for the experiment using pure water are shown in Figure S2 as an example.

To evaluate the mechanisms of the effects of reverse salt flux on DBP transport, Pearson's and Spearman's tests were conducted using Minitab 19. These tests examined the correlation between the change of DBP permeance by reverse salt flux, quantified by the ratio between DBP permeance in FO experiments and that in diffusion cell test using Milli-Q water ($B_{FO}/B_{diffusion\ cell,DI}$), and the molecular size (molecular volume) or hydrophobicity (Log K_{ow}) of the DBPs. Pearson's r measures the linear relationship between two variables, while Spearman's ρ is a nonparametric (monotonic) measure of rank correlation between two variables. The significance level α was set at 0.05. When p value from these tests are less than 0.05, a significant positive (r or $\rho > 0$) or negative (r or $\rho < 0$) correlation is present.

2.4. DBP Sorption Test

Batch experiments were conducted to evaluate the sorption of halogenated DBPs to Aquaporin membrane and polysulfone beads (the material of the Aquaporin support layer). An Aquaporin membrane coupon (0.255 g, 35 cm^2) or 2 g polysulfone beads were added to 20 mL solutions containing 50 $\mu g \cdot L^{-1}$ of each halogenated DBP. To test the "salting-out" effect, sorption tests were conducted in Milli-Q water or 1 M NaCl. Controls were set up with the same DBP concentration and water matrix but without membrane or polysulfone beads. Aqueous samples were collected at 17, 24, and 41 h and analyzed for DBP concentrations. DBP sorption was calculated based on a mass balance approach, with details shown in Text S2.

2.5. DBP Analysis

Samples were raised to 30 mL using Milli-Q water prior to solvent extraction for DBP analysis. For the analysis of halogenated DBPs, the 30 mL-samples were spiked with the internal standard 1,2-dibromopropane (10 $\mu g \cdot L^{-1}$) and mixed with 2 mL MtBE and 10 g sodium sulfate. The extracts were analyzed by gas chromatography-electron capture detector (GC-ECD, Agilent 7890B-63Ni ECD) with an HP-5 column using a previously reported method (Xu et al. 2020). For the analysis of nitrosamines, the 30 mL-samples were spiked with deuterated d6-NDMA as an internal standard and extracted using 2 mL DCM. The extracts were analyzed using gas chromatography-mass spectrometry (Agilent 7890B GC-240 Ion Trap MS) with a VF-5 ms column using a previously reported method (Xu et al. 2018).

3. Modified Solution-Diffusion Model

In the conventional solution-diffusion (SD) model, DBP permeance through membranes can be calculated using the equation 2 (Kong et al. 2015):

$$\frac{1}{B_{SD}} = \frac{1}{B_{AL}^{DI}} + \frac{S}{D_{DBP}} \quad (2)$$

where B_{SD} ($m \cdot s^{-1}$) is the DBP permeance predicted using the SD model; B_{AL}^{DI} ($m \cdot s^{-1}$) is the DBP permeance through the active layer in the absence of reverse salt flux (superscript "DI" refers to Milli-Q water); S (m) is the structure parameter of the membrane; and D_{DBP} ($m^2 \cdot s^{-1}$) is the diffusion coefficient of an individual DBP in Milli-Q water. The detailed derivation is described in Text S3.

To improve the prediction of DBP transport in FO, steric hindrance in the active layer and sorption in the support layer were incorporated into the SD model to account for the effects of reverse salt flux. Through the derivation described in Text S3, equation 3 can be obtained for a modified solution-diffusion (M-SD) model:

$$\frac{1}{B_{M-SD}} = \frac{1}{B_{AL}^{S}} + \frac{S \cdot R_r}{D_{DBP}} \quad (3)$$

where $B_{M\text{-}SD}$ ($m \cdot s^{-1}$) is the DBP permeance through FO membrane predicted using the M-SD model; B_{AL}^{S}($m \cdot s^{-1}$) is the DBP permeance through the active layer with the superscript "S" indicating the consideration of the free volume occupied by draw solutes; and R_r (dimensionless) is the retardation factor resulted from DBP sorption in the support layer. The modeling in this study focuses on NaCl as the draw solute, for which both steric hindrance and sorption exert effects on DBP transport (discussion in section 4.2 below). The model error that refers to the relative difference between the permeance predicted by the M-SD or SD model and the experimental value was calculated using equation 4:

$$Error = \frac{Modeled\ Value - Experimental\ Value}{Experimental\ Value} \times 100\% \quad (4)$$

The structure parameter S was obtained by solving the water flux equation in FO experiments (Phillip et al. 2010):

$$J_w = A\pi_{D,b} \exp(-\frac{J_w S}{D_S}) \quad (5)$$

where J_w ($m^3 \cdot m^{-2} \cdot s^{-1}$) is the water flux; A ($m^3 \cdot m^{-2} \cdot s^{-1} \cdot bar^{-1}$) is the water permeance of the membrane; $\pi_{D,b}$ (bar) is the osmotic pressure of the bulk draw solution; and D_S ($m^2 \cdot s^{-1}$) is the binary diffusion coefficient of the draw solute (for NaCl, $D_S = 1.61 \times 10^{-9}$ $m^2 \cdot s^{-1}$ (Phillip et al. 2010)). D_S values of the three draw solutes are shown in Table S4. The external concentration polarization for NaCl was not considered in this equation because the external concentration polarization factor was close to 1 in our experiments (β = 0.997–0.999; calculated as described in our previous study (Xu et al. 2018)). By solving equation 5 using the results from FO experiments with different draw

NaCl concentrations, S was calculated to be 179 μm for the Aquaporin membrane used in this study.

The diffusion coefficient of each DBP, D_{DBP} ($m^2 \cdot s^{-1}$), was predicted using the U.S. EPA's WATER9 software (EPA 2001):

$$D_{DBP} = 1.518\left(\frac{T}{298.16}\right)\left(\frac{MW}{\rho}\right)^{-0.6} \times 10^{-8} \quad (6)$$

where T (K) is the temperature (293.16 K in this study); MW ($g \cdot mol^{-1}$) is the molecular weight of the DBP; and ρ ($g \cdot L^{-1}$) is the density of the DBP. Table S2 shows the diffusion coefficient of all DBPs. The values of B_{AL}^{S} and R_r were calculated or experimentally determined as described in the following sections.

3.1. Determination of B_{AL}^{S}

The SD model considers the polyamide active layer as "nonporous," but recent studies showed that this dense layer contains interconnected pore-like "microvoids," (Wang et al. 2014, Xie et al. 2018) and that the permeance of DBP through the active layer can be influenced by the effective average pore radius (r_p, nm) in the Aquaporin membrane (Xu et al. 2018):

$$B_{AL} \sim \left(1 - \frac{r_{DBP}}{r_p}\right)^2 \quad (7)$$

where r_{DPB} (nm) is the molecular radius of the DBP (see Table S2); and B_{AL} ($m \cdot s^{-1}$) is the DBP permeance through the active layer. Hence, DBP permeance through the active layer under a given reverse salt flux can be calculated as:

$$\frac{B_{AL}^{S}}{B_{AL}^{DI}} = \left(\frac{1 - \frac{r_{DBP}}{r_p^S}}{1 - \frac{r_{DBP}}{r_p^{DI}}} \right)^2 \quad (8)$$

where r_p^S (nm) and r_p^{DI} (nm) are the effective average pore radii in the presence and absence of the salt, respectively, with the calculation described in Text S4. The prediction was not conducted for three nitrosamines, *N*-nitrosopiperidine, *N*-nitrosodipropylamine, and *N*-nitrosodibutylamine, because their molecular radii (r_{DPB} = 0.300–0.346 nm; see Table S2) are larger than the r_p^S (0.297 nm (Xu et al. 2018)) in the presence of the salt with 1 M NaCl as the draw solution.

The B_{AL}^{DI} of DBPs was determined using the diffusion cell test in Milli-Q water and an equation derived from equation 3:

$$\frac{1}{B_{AL}^{DI}} = \frac{1}{B_{diffusion\ cell,DI}} - \frac{S \cdot R_r}{D_{DBP}} \quad (9)$$

where $B_{diffusion\ cell,DI}$ is DBP permeance through the entire membrane in diffusion cell in Milli-Q water as defined in equation.

3.2. Determination of R_r

The retardation factor for DBP diffusion in the support layer was calculated using equation 10 that was developed for a porous ultrafiltration membrane (Clark and Lucas 1998):

$$R_r = \varepsilon + K_{DBP}^{MSL} \quad (10)$$

where ε is the porosity of the support layer (65% for the Aquaporin membrane used in this study (Sahebi et al. 2019)); and K_{DBP}^{MSL} (dimensionless) is the thickness-averaged partitioning coefficient for a DBP between the support layer and the aqueous solution, with superscript MSL denoting membrane support layer.

The salting-out effect, the enhancement of DBP sorption in the support layer via hydrophobic interaction, can be described using equation 11 (Burant et al. 2017):

$$\mathrm{Log}\frac{K_{DBP,Salt}^{MSL}}{K_{DBP,DI}^{MSL}} = k_{DBP}^{Salt}\cdot C^{S} \tag{11}$$

where $K_{DBP,Salt}^{MSL}$ and $K_{DBP,DI}^{MSL}$ are the partitioning coefficients (dimensionless) of DBPs, defined as the ratio of the equilibrium DBP concentration in the support layer to that in a saline solution and Milli-Q water, respectively; k_{DBP}^{Salt} (M^{-1}) is the Setschenow constant; and C^{S} (M) is the corresponding salt concentration of the saline solution. Within the support layer, the extent of the salting-out effect is influenced by the salt concentration profile (Figure S3), and therefore K_{DBP}^{MSL} in equation 10 for FO is a thickness-averaged partitioning coefficient.

3.2.1. Draw Solute Concentration Profile in Support Layer

The salt concentration at a particular position within the support layer and that at the interface between the support and active layers can be calculated using the equations developed in a previous study (Phillip et al. 2010):

$$C_z^S = \frac{\exp(\frac{J_w S}{D_S} z)\cdot(C_D^S - C_i^S) + \exp(\frac{J_w S}{D_S})\cdot C_i^S - C_D^S}{\exp(\frac{J_w S}{D_S}) - 1} \tag{12}$$

$$C_i^S = \frac{J_S\left[\exp(\frac{J_w S}{D_S}) - 1\right] + J_w\cdot C_D^S}{J_w \exp(\frac{J_w S}{D_S})} \tag{13}$$

where C_z^S, C_i^S, and C_D^S (M) are the salt concentrations in the support layer at position z, at the interface between the support and active layers (i.e., $z = 0$), at the interface between the support layer and draw reservoir (i.e., $z = 1$), respectively; and J_S ($mol\cdot m^{-2}\cdot s^{-1}$) is the reverse salt flux. The

values of C_D^S (M) are 0.19, 0.45, or 0.85 M after accounting for the dilution of draw reservoir in our FO experiments with initial NaCl concentrations of 0.2, 0.5, or 1 M, respectively. The thickness-averaged K_{DBP}^{MSL} can be calculated using the following equation:

$$K_{DBP}^{MSL} = \int_0^1 \left(K_{DBP,DI}^{MSL} \cdot 10^{k_{DBP}^{Salt} \cdot C^S(z)} \right) dz \tag{14}$$

3.2.2. Determination of $K_{DBP,DI}^{MSL}$ and k_{DBP}^{Salt} by Contact Angle Measurement

The $K_{DBP,DI}^{MSL}$ and $K_{DBP,Salt}^{MSL}$ were calculated based on the DBP-membrane interaction in Milli-Q water and saline solutions, respectively:

$$K_{DBP,j}^{MSL} = \exp\left[-\left(\frac{\Delta G_{DBP,j}^{MSL}}{k \cdot T} \right) \right] \tag{15}$$

where $\Delta G_{DBP,j}^{MSL}$ (J) is the free energy of the interaction between a DBP molecule in the solution and the membrane support layer, with subscript j = DI or Salt to denote Milli-Q water or saline solution, respectively; and k is the Boltzmann constant (1.38×10^{-23} J·K^{-1}). $\Delta G_{DBP,j}^{MSL}$ was estimated using the surface tension components of the membrane support layer, water, and DBP (van Oss 2007):

$$\Delta G_{DBP,j}^{MSL} = 2A_{DBP} \left[\begin{array}{l} \sqrt{\gamma_{DBP}^{LW}\gamma_j^{LW}} + \sqrt{\gamma_{MSL}^{LW}\gamma_j^{LW}} - \sqrt{\gamma_{MSL}^{LW}\gamma_{DBP}^{LW}} - \gamma_j^{LW} \\ + \sqrt{\gamma_j^+}\left(\sqrt{\gamma_{DBP}^-} + \sqrt{\gamma_{MSL}^-} - \sqrt{\gamma_j^-}\right) \\ + \sqrt{\gamma_j^-}\left(\sqrt{\gamma_{DBP}^+} + \sqrt{\gamma_{MSL}^+} - \sqrt{\gamma_j^+}\right) - \sqrt{\gamma_{DBP}^+\gamma_{MSL}^-} - \sqrt{\gamma_{DBP}^-\gamma_{MSL}^+} \end{array} \right] \tag{16}$$

where A_{DBP} (m^2) is the contact area between a DBP molecule and the membrane and was calculated using $\pi r_{DBP}^2/2$ (Bhattacharjee et al. 1996), where r_{DBP} (m) is the molecular radius of the DBP molecule; γ_j^{LW} (J·m^{-2}) is the apolar (Lifshitz-van der Waals) surface tension component; and γ_j^+ (J·m^{-2}) and γ_j^- (J·m^{-2}) are the polar (Lewis acid-base) electron-accepting and electron-donating

surface tension components, respectively. The subscripts "DBP" and "MSL" represent DBP and the membrane support layer, respectively.

The specific surface tension components of the membrane and DBP liquid are linked to the contact angle (θ) of liquid droplets (L) on a solid surface (S) via the Young-Dupré equation (van Oss 2007):

$$\left(1+\cos\theta\right)\left(\gamma_L^{LW}+2\sqrt{\gamma_L^+\gamma_L^-}\right)= 2\left(\sqrt{\gamma_S^{LW}\gamma_L^{LW}}+\sqrt{\gamma_S^+\gamma_L^-}+\sqrt{\gamma_S^-\gamma_L^+}\right) \quad (17)$$

The γ_S^{LW}, γ_S^+, and γ_S^- values for the membrane support layer (i.e., γ_{MSL}^{LW}, γ_{MSL}^+, and γ_{MSL}^-) were obtained by solving equation 17 using the contact angles of a nonpolar solvent (diiodomethane) and two polar solvents (glycerol and water) on the support layer (Van Oss 2006). Similarly, the γ_{DBP}^{LW}, γ_{DBP}^+, and γ_{DBP}^- values for two DBPs, NDMA and DCAN, were determined using the contact angles of the respective pure liquid on three reference surfaces polytetrafluoroethylene (PTFE), quartz, and cross-linked poly(ethylene glycol). Pure NDMA and DCAN are acutely toxic, flammable, and carcinogenic, and hence should be handled carefully following instructions on the safety data sheet. The γ_{DBP}^{LW}, γ_{DBP}^+, and γ_{DBP}^- values for chloroform (TCM) (Van Oss 2006) and bromoform (TBM) (Janczuk et al. 1993) are available from the literature. The γ_j^{LW}, γ_j^+, and γ_j^- values for the support layer of the Aquaporin membrane and the four DBPs are summarized in Table 1. For these four DBPs, $K_{DBP,DI}^{MSL}$ values were calculated using equations 15 and 16.

In order to obtain the Setschenow constants k_{DBP}^{Salt} for these four DBPs, the surface tension components of 8 NaCl solutions (0.1–3 M) were determined using their contact angles on the three reference surfaces. The $\Delta G_{DBP,Salt}^{MSL}$ values for the interaction energy between DBP and the membrane support layer in these NaCl solutions were calculated using equation 16, and the $K_{DBP,Salt}^{MSL}$ values in the corresponding NaCl solutions were calculated using equation 15. The slope

of the linear regression of Log ($K^{MSL}_{DBP,Salt}/K^{MSL}_{DBP,DI}$) to C^S gives the Setschenow constant $k_{DBP}{}^{Salt}$ for each DBP (equation 11), as shown in Figure 1.

3.2.3. $K^{MSL}_{DBP,DI}$ and k^{Salt}_{DBP} Values for Other DBPs

The method to derive $K^{MSL}_{DBP,DI}$ and k^{Salt}_{DBP} described in 3.2.2 is limited to the availability of pure compounds and involves the handling of highly toxic substances. To expand the application of M-SD model to the other 9 DBPs investigated in this study, their partitioning coefficient and Setschenow constants were estimated using methods based on their molecular properties (Ni and Yalkowsky 2003, Vaes et al. 1998). Vaes et al. (1998) used a regression method to establish the relationship between the partitioning coefficients of organic compounds and their molecular properties including MV (the molecular volume, Å^3), K_{ow} (the octanol/water partitioning coefficient, dimensionless), ε_{HOMO} (the energy level of the highest occupied molecular orbital, eV), ε_{LUMO} (the energy level of the lowest unoccupied molecular orbital, eV), Q^- (the most negative charge on any non-hydrogen atom, a.u.), and Q^+ (the most positive charge on any hydrogen atom, a.u.). To adapt this method to predict the partitioning coefficient $K^{MSL}_{DBP,DI}$, we first selected 22 reference organic compounds with available surface tension components in the literature (Botton et al. 2012, De Ridder et al. 2013, Van Oss 2006) (Table S5) and calculated their K^{MSL}_{DI} (dimensionless) values for the support layer of the Aquaporin membrane using equations 15 and 16. Subsequently, a multivariate regression model describing the relationship between the molecular properties of the 22 organic compounds and their Log K^{MSL}_{DI} for the support layer of the Aquaporin membrane was obtained:

$$\begin{aligned}\text{Log}\, K^{MSL}_{DI} &= 0.516 + 0.0147\varepsilon_{HOMO} - 0.0538\varepsilon_{LUMO} - 0.207Q^- \\ &-1.350\, Q^+ + 0.000295MV + 0.1767\text{Log}\, K_{ow} \quad R^2 = 0.94\end{aligned} \tag{18}$$

where K_{DI}^{MSL} (dimensionless) is the partitioning coefficient of an organic compound between the support layer of the Aquaporin membrane and Milli-Q water. The $K_{DBP,DI}^{MSL}$ of DBPs, similar to the K_{DI}^{MSL} of the reference compounds, was then calculated using equation 18 based on the molecular properties of DBPs. The values of ε_{HOMO}, ε_{LUMO}, Q^-, and Q^+ for all 22 reference compounds and 13 DBPs were estimated using PM6 method through the semi-empirical quantum chemistry program MOPAC2016 (Stewart 2016). The values of MV and Log K_{ow} were obtained from PubChem database (Kim et al. 2016).

The Setschenow constant of all DBPs in NaCl solutions was predicted using equation 19, an empirical equation initially developed for 101 organic compounds (Ni and Yalkowsky 2003):

$$k_{DBP}^{Salt} = 0.04 \text{Log } K_{ow} + 0.114 \quad (19)$$

The $K_{DBP,DI}^{MSL}$ and k_{DBP}^{Salt} values for TCM, TBM, DCAN, and NDMA determined from these regression models (equations 18 and 19, respectively) are similar to those obtained using contact angle measurement (Table 2), validating them for estimating the $K_{DBP,DI}^{MSL}$ and k_{DBP}^{Salt} values of the other 9 DBPs investigated in this study.

4. Results and Discussion

4.1. Effects of Reverse Salt Flux on DBP Rejection and Permeance

Over the course of the FO experiment, the rejection of all DBPs by Aquaporin membrane exhibited a small initial decline and then stabilized after 150–600 mL of water permeated through the membrane (Figure S4 for four DBPs as examples). The stabilized rejection is used in the discussion for the rest of the manuscript. Figure 2a shows the rejection of the sixteen DBPs under a water flux of 3.0–4.0 $L \cdot m^{-2} \cdot h^{-1}$ with three different compounds NaCl, $MgSO_4$, and glucose as draw solutes. For halogenated DBPs, the rejection was highest when NaCl was used as the draw solute, followed by glucose and then $MgSO_4$. Two of the trihalomethanes TCM and DCBM even

exhibited negative rejection with $MgSO_4$ as the draw solute. Based on the solution-diffusion mechanism (Xie et al. 2018), DBP transport in FO is mainly governed by diffusion and is independent on water flux. In cases where water flux was low (e.g., 3.0 $L \cdot m^{-2} \cdot h^{-1}$ with 1 M $MgSO_4$ as the draw solution), the faster transport of DBP than water would lead to a DBP to water flux ratio (equations S1 and S2) greater than the average DBP concentration in the feed solution, resulting in a negative rejection (equation S3). The dependence of the rejection of halogenated DBPs on draw solutes is similar to that previously reported for PPCPs, i.e., NaCl provided the highest PPCP rejection, followed by glucose and $MgSO_4$ (Xie et al. 2018). Because the three draw solutions imposed a range of reverse salt flux (6.8–35.8 $mmol \cdot m^{-2} \cdot h^{-1}$), our results further support the previous observation that reverse salt flux is an important factor influencing the forward transport of organic solutes (Xie et al. 2012). In contrast, most nitrosamines, except the smallest compound NDMA, did not show a substantial difference in rejection when different draw solutes were used (Figure 2a).

DBP permeance from the above experiments, as well as those from experiments using NaCl solutions of different concentrations (rejection values shown in Figure 2b), was calculated to further assess the effects of reverse salt flux on DBP transport (Figure 3). The five different draw solutions resulted in a range of reverse salt flux (6.8–60.3 $mmol \cdot m^{-2} \cdot h^{-1}$, Table S4). The permeance of halogenated DBPs (Figures 3a and 3b) decreased with the increase of reverse salt flux. For example, the permeance of TCM and DCAN decreased from 1.00 $\mu m \cdot s^{-1}$ to 0.81 $\mu m \cdot s^{-1}$ and from 0.76 $\mu m \cdot s^{-1}$ to 0.66 $\mu m \cdot s^{-1}$, respectively, when reverse salt flux increased from 6.8 to 60.3 $mmol \cdot m^{-2} \cdot h^{-1}$. In contrast, such a trend was not observed for nitrosamines, the permeance of which remained approximately constant across the range of reverse salt flux tested (Figure 3c). Previous studies hypothesized that the effect of reverse salt flux can be attributed to the steric

hindrance introduced by the draw solute molecules on the forward transport of organic molecules (Xie et al. 2012). In other words, one would expect that organic molecules of similar sizes to be impacted by reserve salt flux similarly. This, however, does not apply to our DBP results. For example, DCAN and NDMA feature similar molecular radii around 0.259 nm, but only DCAN showed a decrease in permeance with increasing reverse salt flux. The different effects of reverse salt flux on the rejection and permeance between halogenated DBPs and nitrosamines, despite their similar molecular size, suggest that mechanisms beyond the hindrance effect are at play.

It should be mentioned that convection can also play a role in the transport of organic contaminants (Xie et al. 2014), which can generate confounding factors for the effect of reverse salt flux, because varying reverse salt flux is often accompanied with different water fluxes. However, as shown in Table S10, even at the highest water flux (8.1 $L \cdot m^{-2} \cdot h^{-1}$) tested in this study (i.e., maximal convection), convection only accounted for less than 10% of total flux for all DBPs, indicating that its role was overall minor in this study.

4.2. Mechanistic Investigation of the Reverse Salt Flux Effects

4.2.1. Steric Hindrance

The steric hindrance for the forward transport of organic molecules can result from the countermovement of draw solute molecules or simply from their presence in the membrane active layer. To differentiate these two possibilities, experiments were conducted in diffusion cells, where there is no movement of draw solute molecules. As shown in Figure 4, DBP permeance was much lower in NaCl solutions than that in pure water; the higher the NaCl concentration, the lower the DBP permeance. These results indicate that the presence of NaCl in the membrane (i.e., without movement) already hinders DBP transport.

417 According to the steric hindrance theory, draw solutes with similar radii as the membrane
418 effective pore radius could occupy the free space in the membrane active layer and thereby hinder
419 the transport of organic molecules with similar molecular radii (Scheme S1a). In other words, for
420 organic molecules smaller than the draw solutes, their transport should be less hindered (Scheme
421 S1b). This hypothesis was tested by examining the relationship between the drop in DBP
422 permeance in the presence of draw solutes and the size of DBPs (Figure 5). The decrease in DBP
423 permeance is represented as the ratio of the DBP permeance in FO experiments with various draw
424 solutes to the DBP permeance in diffusion cell experiments with pure water. Pearson's (linear,
425 parametric) and Spearman's (monotonic, non-parametric) correlation tests show that the drop in
426 DBP permeance in the presence of draw solutes $MgSO_4$ or glucose inversely correlated with the
427 molecular volume of DBPs, but such a correlation was not observed for NaCl. These results
428 indicate that the steric hindrance by the larger draw solutes $MgSO_4$ or glucose plays an important
429 role in hindering the forward DBP transport in FO, but other physicochemical processes may
430 contribute to the hindered DBP transport by the smaller draw solute NaCl.

431 **4.2.2. Retardation of DBP Diffusion in the Support Layer**

432 The role of the support layer in the presence of draw solutes on DBP transport has not been
433 previously examined. Compared with the active layer, the support layer has an open structure and
434 hence is not likely to restrict the movement of DBP molecules. However, it can serve as a sorption
435 media for organic compounds. Accordingly, the relationship between the drop in DBP permeance
436 in the presence of draw solutes and the hydrophobicity of DBPs (Log K_{ow}) was analyzed (Figure
437 6). In contrast to the results observed for molecular volume (Figure 5), Figure 6 shows that the
438 drop in DBP permeance due to the presence of NaCl inversely correlated with the Log K_{ow} of
439 DBPs, but such a correlation was not observed for $MgSO_4$ or glucose. This can be rationalized by

440 the larger size of $MgSO_4$ and glucose than NaCl, which results in a dominating steric hindrance
441 effect in the active layer, and, in the case of glucose, the lack of ionic charge to induce the "salting-
442 out" effect in the support layer.

443 The wastewater-relevant, low DBP concentrations (10–20 $\mu g \cdot L^{-1}$) used in the feed for the
444 FO experiments render it challenging to quantify the amount of DBP in the Aquaporin membrane
445 using desorption tests. Accordingly, we conducted sorption experiments in batch systems using
446 Aquaporin membrane coupons or polysulfone beads (the material of the support layer) in Milli-Q
447 water or 1 M NaCl solution for halogenated DBPs (Figure S5). In the presence of Aquaporin
448 membrane or polysulfone beads, DBP concentrations in the aqueous phase declined initially, and
449 then reached a plateau by 41 h, by when 70%–98% and 11%–52% of the total DBP mass
450 partitioned into the Aquaporin membrane coupon and polysulfone beads, respectively. Higher
451 sorption occurred in 1 M NaCl solution than in Milli-Q water. Among different DBPs, the extent
452 of sorption on Aquaporin membrane or polysulfone beads (in Milli-Q water) correlated with the
453 partitioning coefficient $K_{DBP,DI}^{MSL}$ value of the DBPs (Figures S6a and S6b). Additionally, the
454 enhancement of sorption in 1 M NaCl solution compared with that in Milli-Q water correlated with
455 the Setschenow constant k_{DBP}^{Salt} of the DBPs (Figures S6c and S6d), supporting the "salting-out"
456 effects. Overall, these results support that sorption of DBPs in the support layer, especially in the
457 presence of the high concentration of salts, can contribute to the retardation of DBP transport in
458 FO.

459 **4.3. Modelling DBP Transport in FO**

460 **4.3.1. Steric Hindrance in the Active Layer**

461 The effective pore radius r_p^S and the associated DBP permeance through the active layer
462 B_{AL}^S are shown in Table 3 for four representative DBPs. As reverse NaCl flux increased, both r_p^S

and B_{AL}^{S} decreased. When reverse NaCl flux increased from 0 to 60.3 mmoL·m^{-2}·h^{-1}, r_p^S decreased from 0.305 to 0.297 nm; this seemingly small change in r_p^S (<3% decrease) resulted in a substantial decrease in B_{AL}^{S} by 26%–38%. Additionally, the decrease in B_{AL}^{S} is more pronounced for larger DBPs: TBM (r_{DBP} = 0.271 nm) exhibited a greater decrease (38%) in B_{AL}^{S} than the other three DBPs (r_{DBP} = 0.256–0.259 nm) (26%–29% decrease). Figure 7 simulates the change in B_{AL}^{S} due to the presence of NaCl as a function of DBP size, showing that the presence of salt has a stronger effect on suppressing the permeance of larger DBPs through the active layer. Beyond DBPs, this trend may be applicable to other neutral organic molecules with radii smaller than the effective pore radius of the membrane in the presence of draw solutes.

4.3.2. Retarded Diffusion in the Support Layer

The values of the retardation factor R_r for all DBPs are shown in Table 4. For all DBPs, the higher the reverse NaCl flux, the greater the value of R_r, indicating a stronger retardation effect in the support layer. Additionally, the increase in R_r accompanied by increasing reverse NaCl flux is greater for DBPs with higher hydrophobicity. For example, R_r of TBM (Log K_{ow} = 2.40) increased by 42% when reverse NaCl flux increased from 0 to 60.3 mmoL·m^{-2}·h^{-1}, while NDMA (Log K_{ow} = -0.64) featured only 7% increase in R_r. This dependence is consistent with the results observed in Figure 6, where a stronger effect of reverse NaCl flux was observed on the permeance of DBPs with higher hydrophobicity.

4.3.3. Predicting DBP Permeance with the Modified Solution-Diffusion Model

The DBP permeance and rejection determined from FO experiments were compared with those predicted using the conventional solution-diffusion (SD) model or the modified solution-diffusion (M-SD) model. As shown in Figure 8, for all halogenated DBPs (trihalomethanes, haloacetonitriles, haloketones), the M-SD model more accurately predicted DBP permeance and

rejection than the SD model, and the improved accuracy of the M-SD model is more pronounced at higher reverse salt flux. The model error calculated by equation 4 was compared between the M-SD and SD models. For trihalomethanes, a group of DBPs regulated by U.S. EPA, the M-SD model predicted their permeance with error of 3%–20% at the low reverse NaCl flux of 20.9 $mmol \cdot m^{-2} \cdot h^{-1}$ (Figure 8a), better than the SD model (9%–30% error). At the high reverse NaCl flux of 60.3 $mmol \cdot m^{-2} \cdot h^{-1}$, the errors of the M-SD and SD models in predicting trihalomethanes permeance were -2%–121% and 28%–238% (Figure 8b), respectively. For haloacetonitriles, a group of DBPs recently shown to contribute to the majority of the toxicity in recycled wastewater (Lau et al. 2020, Zeng et al. 2016), the M-SD model provided accurate prediction for their permeance (2%–13% and -10%–25% errors at low and high reverse NaCl flux, respectively), a significant improvement from the SD model (10%–22% and 20%–91% errors). For haloketones, the M-SD and SD model predicted the permeance with errors of -89%–-35% and 10%–150%, respectively, at the high reverse NaCl flux.

In contrast, for the four nitrosamines, the M-SD model underestimated their permeance. At the high reverse NaCl flux, the error of the M-SD model in predicting permeance was -26% for NDMA and -37%–-94% for the other three nitrosamines (Figure 8b), whereas the error of the SD model was -1%–33% for these nitrosamines. NDMA, the smallest nitrosamine with high hydrophilicity (Log K_{ow} = -0.64), can possibly be transported through convection, but the low contribution of convection to total NDMA flux in our experiments (< 3%, Table S10) suggests that the prediction error of the M-SD model for NDMA is attributed to other factors. As for the other three nitrosamines, the poor performance of the M-SD model may be attributed to the large size of these compounds, with radius (0.278–0.295 nm) close to the effective pore radius r_p^S of the active layer in the presence of salt. As shown in Figure 7, the effect of steric hindrance, reflected

509 by the ratio of B_{AL}^{S} to B_{AL}^{DI}, is extremely sensitive to DBP radii as they approach r_p^S. In reality, rather
510 than a uniform pore size (r_p^S), the effective pores in the active layer likely feature a range of sizes
511 (Fang et al. 2014), with larger "pores" available for the transport of large DBPs. This pore size
512 distribution is not considered in either the M-SD or SD model, but M-SD model is more affected
513 due to the consideration of pore restriction by draw salt in the active layer.

514 For halogenated DBPs, the relative importance of steric hindrance versus retarded diffusion
515 in contributing to the effects of reverse salt flux on DBP permeance is shown in Figure 9 for three
516 representative compounds. Between TCM and DCAN with similar molecular sizes (r_{DBP} = 0.256–
517 0.259 nm), the more hydrophobic TCM (Log K_{ow} = 1.97) is more affected by retarded diffusion in
518 the support layer than by steric hindrance in the active layer, while the less hydrophobic DCAN
519 (Log K_{ow} = 0.29) is more affected by steric hindrance. For dibromochloromethane (DBCM), a
520 relatively large and hydrophobic DBP, steric hindrance and retarded diffusion contributed
521 similarly.

522 **4.3.4. Model Limitations**

523 Although the M-SD model significantly improved the prediction of the permeance of
524 halogenated DBPs, a few limitations should be acknowledged. First, the pore size distribution of
525 the active layer is not captured by the use of effective pore radius r_p^S in the model. As a result, the
526 M-SD model cannot predict the permeance of DBPs with radii larger than r_p^S, such as *N*-
527 nitrosopiperidine, *N*-nitrosodipropylamine, and *N*-nitrosodibutylamine (Tables 3 and S2). Even for
528 DBPs with radii smaller than, but close to, r_p^S, the M-SD model significantly underestimated the
529 permeance, such as for *N*-nitrosodiethylamine (r_{DBP} = 0.295 nm) (Figure S7). This limitation,
530 however, may not be critical for application in wastewater recycling, because these large DBPs
531 generally have high rejection (e.g., > 85% with 1 M NaCl as the draw solution, Figure 2) and have

been shown to contribute to relatively low health risks in full-scale wastewater recycling operation (Zeng et al. 2016). Second, the M-SD model does not consider the convection process. Although convection contributed to less than 10% of the total DBP flux across experiments conducted in this study (Table S10), its role can be substantial at higher water fluxes, warranting further consideration in future studies. Third, further improvement of the M-SD model may consider the depth heterogeneity of the support layer when determining the effect of retarded diffusion on hydrophobic compounds. The polysulfone layer is usually heterogeneous in depth (Breitbach et al. 1991), suggesting that the partitioning coefficient determined from the surface of the support layer may not fully represent the partitioning in the entire support layer. Because retarded diffusion is particularly important for the more hydrophobic compounds, accurate determination of their partitioning coefficients with the support layer is critical for predicting their permeance in the presence of reverse salt flux. For example, the only three halogenated DBPs (i.e., dichlorobromomethane, dibromochloromethane, and bromoform), whose permeance values were not accurately predicted by the M-SD model (see Figure 8), had the highest hydrophobicity among the halogenated DBPs tested (Log K_{ow} >2). Lastly, the M-SD model has not incorporated the effects of organic fouling. Organic fouling can hinder the diffusion of draw solutes from the active layer to the feed solution and therefore elevate draw solute concentrations in the active layer (Lee et al. 2010). As a result, the steric hindrance caused by reverse salt flux on DBP transport is expected to be enhanced by the organic fouling. Future research is needed to systematically evaluate the varying effects of the different types of organic fouling that are relevant to wastewater recycling on the transport of organic contaminants and to incorporate them into transport models.

5. Conclusion

554 This study evaluated the effects of reverse salt flux on the forward transport of 16 neutral
555 DBPs in FO, including 9 halogenated DBPs (4 trihalomethanes, 3 haloacetonitriles, and 2
556 haloketones) and 7 nitrosamines. Using three draw solutes NaCl, $MgSO_4$, and glucose, we
557 observed that the higher the reverse salt flux, the lower the DBP permeance and hence the higher
558 the DBP rejection by the Aquaporin membrane. This effect of reverse salt flux was stronger for
559 halogenated DBPs than for nitrosamines. Correlation analysis combining results from FO and
560 diffusion cell experiments showed that the steric hindrance in the active layer contributed to the
561 effects of reverse salt flux for $MgSO_4$ and glucose, while the retarded diffusion in the support layer
562 played a major role for NaCl.

563 This study is one of the first attempts to incorporate the effects of reverse salt flux for the
564 forward transport of organic compounds in FO transport models. We modified the conventional
565 solution-diffusion (SD) model by incorporating both steric hindrance and retarded diffusion to
566 predict the DBP permeance under low and high reverse salt fluxes. The steric hindrance in the
567 active layer was reflected by the effective pore radius (r_p^S) after accounting for the free volumes
568 occupied by draw solutes. The retardation factor in the support layer was estimated using the
569 partitioning coefficient of DBPs between the support layer and water ($K_{DBP,DI}^{MSL}$) as well as the
570 Setschenow constant representing the salting-out effect (k_{DBP}^{Salt}). Our modified SD (M-SD) model
571 predicted the permeance of halogenated DBPs better than the conventional SD model. Specifically,
572 the permeance of haloacetonitriles, a group of high-priority DBPs in wastewater recycling, was
573 predicted by the M-SD model with less than 25% error from the experimental observation. Steric
574 hindrance is the dominant mechanism for the reverse salt flux effect for large DBPs, while retarded
575 diffusion contributed more for hydrophobic DBPs. The M-SD model underestimated the
576 permeance of nitrosamines, presumably due to the limitation that the M-SD model did not consider

convection as a transport mechanism (for hydrophilic compound) or the effective pore size distribution of the membrane active layer.

Acknowledgment

The research was supported by the National Science Foundation (1652412). There is no conflict of interest to declare.

Appendix A. Supplementary material

583 **References**

584 Alturki, A.A., McDonald, J.A., Khan, S.J., Price, W.E., Nghiem, L.D., Elimelech, M., 2013.
585 Removal of trace organic contaminants by the forward osmosis process. Sep. Purif.
586 Technol. 103, 258-266.
587 Bhattacharjee, S., Sharma, A., Bhattacharya, P.K., 1996. Estimation and influence of long range
588 solute. Membrane interactions in ultrafiltration. Ind. Eng. Chem. Res. 35, 3108-3121.
589 Botton, S., Verliefde, A.R., Quach, N.T., Cornelissen, E.R., 2012. Influence of biofouling on
590 pharmaceuticals rejection in nf membrane filtration. Water Res. 46, 5848-5860.
591 Breitbach, L., Hinke, E., Staude, E., 1991. Heterogeneous functionalizing of polysulfone
592 membranes. Die Angewandte Makromolekulare Chemie: Applied Macromolecular
593 Chemistry and Physics 184, 183-196.
594 Burant, A., Lowry, G.V., Karamalidis, A.K., 2017. Measurement and modeling of setschenow
595 constants for selected hydrophilic compounds in NaCl and $CaCl_2$ simulated carbon storage
596 brines. Accounts Chem. Res. 50, 1332-1341.
597 Cheong, S.I., Kim, B., Lee, H., Rhim, J.W., 2013. Physical adsorption of water-soluble polymers
598 on hydrophobic polymeric membrane surfaces via salting-out effect. Macromol. Res. 21,
599 629-635.
600 Clark, M.M., Lucas, P., 1998. Diffusion and partitioning of humic acid in a porous ultrafiltration
601 membrane. J. Membrane Sci. 143, 13-25.
602 Coday, B.D., Yaffe, B.G.M., Xu, P., Cath, T.Y., 2014. Rejection of trace organic compounds by
603 forward osmosis membranes: A literature review. Environ. Sci. Technol. 48, 3612-3624.
604 D'Haese, A.K.H., 2020. Interactions between feed solutes and inorganic electrolytic draw solutes
605 in forward osmosis. J. Membrane Sci. 597, 117636.

606 Dai, N., Zeng, T., Mitch, W.A., 2015. Predicting n-nitrosamines: N-nitrosodiethanolamine as a
607 significant component of total n-nitrosamines in recycled wastewater. Environ. Sci. Tech.
608 Let. 2, 54-58.
609 De Ridder, D.J., Verliefde, A.R., Schoutteten, K., Van Der Linden, B., Heijman, S.G., Beurroies,
610 I., Denoyel, R., Amy, G.L., Van Dijk, J.C., 2013. Relation between interfacial energy and
611 adsorption of organic micropollutants onto activated carbon. Carbon 53, 153-160.
612 Engelhardt, S., Sadek, A., Duirk, S., 2018. Rejection of trace organic water contaminants by an
613 aquaporin-based biomimetic hollow fiber membrane. Sep. Purif. Technol. 197, 170-177.
614 Fang, Y., Bian, L., Bi, Q., Li, Q., Wang, X., 2014. Evaluation of the pore size distribution of a
615 forward osmosis membrane in three different ways. J. Membrane Sci. 454, 390-397.
616 Ferby, M., Zou, S., He, Z., 2020. Reduction of reverse solute flux induced solute buildup in the
617 feed solution of forward osmosis. Environ. Sci.-Wat. Res.
618 Han, G., Zhang, S., Li, X., Widjojo, N., Chung, T.-S., 2012. Thin film composite forward osmosis
619 membranes based on polydopamine modified polysulfone substrates with enhancements in
620 both water flux and salt rejection. Chem. Eng. Sci. 80, 219-231.
621 Heo, J., Boateng, L.K., Flora, J.R.V., Lee, H., Her, N., Park, Y.G., Yoon, Y., 2013. Comparison
622 of flux behavior and synthetic organic compound removal by forward osmosis and reverse
623 osmosis membranes. J. Membrane Sci. 443, 69-82.
624 Janczuk, B., Chibowski, E., Bruque, J., Kerkeb, M., Caballero, F.G., 1993. On the consistency of
625 surface free energy components as calculated from contact angles of different liquids: An
626 application to the cholesterol surface. J. Colloid Interf. Sci. 159, 421-428.

627 Jang, Y., Cho, H., Shin, Y., Choi, Y., Lee, S., Koo, J., 2016. Comparison of fouling propensity
628 and physical cleaning effect in forward osmosis, reverse osmosis, and membrane
629 distillation. Desalin. Water Treat. 57, 24532-24541.
630 Jin, X., Tang, C.Y., Gu, Y.S., She, Q.H., Qi, S.R., 2011. Boric acid permeation in forward osmosis
631 membrane processes: Modeling, experiments, and implications. Environ. Sci. Technol. 45,
632 2323-2330.
633 Kim, C., Lee, S., Shon, H.K., Elimelech, M., Hong, S., 2012. Boron transport in forward osmosis:
634 Measurements, mechanisms, and comparison with reverse osmosis. J. Membrane Sci. 419-
635 420, 42-48.
636 Kim, S., Thiessen, P.A., Bolton, E.E., Chen, J., Fu, G., Gindulyte, A., Han, L., He, J., He, S.,
637 Shoemaker, B.A., 2016. Pubchem substance and compound databases. Nucleic Acids Res.
638 44, D1202-D1213.
639 Kim, Y., Li, S., Chekli, L., Woo, Y.C., Wei, C.-H., Phuntsho, S., Ghaffour, N., Leiknes, T., Shon,
640 H.K., 2017. Assessing the removal of organic micro-pollutants from anaerobic membrane
641 bioreactor effluent by fertilizer-drawn forward osmosis. J. Membrane Sci. 533, 84-95.
642 Kong, F.X., Dong, L.Q., Zhang, T., Chen, J.F., Guo, C.M., 2018. Effect of reverse permeation of
643 draw solute on the rejection of ionic nitrogen inorganics in forward osmosis: Comparison,
644 prediction and implications. Desalination 437, 144-153.
645 Kong, F.X., Yang, H.W., Wang, X.M., Xie, Y.F.F., 2014. Rejection of nine haloacetic acids and
646 coupled reverse draw solute permeation in forward osmosis. Desalination 341, 1-9.
647 Kong, F.X., Yang, H.W., Wu, Y.Q., Wang, X.M., Xie, Y.F.F., 2015. Rejection of pharmaceuticals
648 during forward osmosis and prediction by using the solution-diffusion model. J. Membrane
649 Sci. 476, 410-420.

650 Lau, S.S., Wei, X., Bokenkamp, K., Wagner, E.D., Plewa, M.J., Mitch, W.A., 2020. Assessing
651 additivity of cytotoxicity associated with disinfection byproducts in potable reuse and
652 conventional drinking waters. Environ. Sci. Technol. 54, 5729-5736.
653 Lee, S., Boo, C., Elimelech, M., Hong, S., 2010. Comparison of fouling behavior in forward
654 osmosis (FO) and reverse osmosis (RO). J. Membrane Sci. 365, 34-39.
655 Lin, S., 2016. Mass transfer in forward osmosis with hollow fiber membranes. J. Membrane Sci.
656 514, 176-185.
657 Linares, R.V., Li, Z., Sarp, S., Bucs, S.S., Amy, G., Vrouwenvelder, J.S., 2014. Forward osmosis
658 niches in seawater desalination and wastewater reuse. Water Res. 66, 122-139.
659 Luo, W., Xie, M., Song, X., Guo, W., Ngo, H.H., Zhou, J.L., Nghiem, L.D., 2018. Biomimetic
660 aquaporin membranes for osmotic membrane bioreactors: Membrane performance and
661 contaminant removal. Bioresource Technol. 249, 62-68.
662 Lutchmiah, K., Verliefde, A.R.D., Roest, K., Rietveld, L.C., Cornelissen, E.R., 2014. Forward
663 osmosis for application in wastewater treatment: A review. Water Res. 58, 179-197.
664 Madsen, H.T., Bajraktari, N., Helix-Nielsen, C., Van der Bruggen, B., Sogaard, E.G., 2015. Use
665 of biomimetic forward osmosis membrane for trace organics removal. J. Membrane Sci.
666 476, 469-474.
667 Mi, B., Elimelech, M., 2010. Organic fouling of forward osmosis membranes: Fouling reversibility
668 and cleaning without chemical reagents. J. Membrane Sci. 348, 337-345.
669 Ni, N., Yalkowsky, S.H., 2003. Prediction of setschenow constants. Int. J. Pharmaceut. 254, 167-
670 172.
671 NRC, 2012. Water reuse: Potential for expanding the nation's water supply through reuse of
672 municipal wastewater, The National Academies Press, Washington, DC.

673 Phillip, W.A., Yong, J.S., Elimelech, M., 2010. Reverse draw solute permeation in forward
674 osmosis: Modeling and experiments. Environ. Sci. Technol. 44, 5170-5176.
675 Qi, S., Wang, R., Chaitra, G.K.M., Torres, J., Hu, X., Fane, A.G., 2016. Aquaporin-based
676 biomimetic reverse osmosis membranes: Stability and long term performance. J.
677 Membrane Sci. 508, 94-103.
678 Qin, M., He, Z., 2014. Self-supplied ammonium bicarbonate draw solute for achieving wastewater
679 treatment and recovery in a microbial electrolysis cell-forward osmosis-coupled system.
680 Environ. Sci. Tech. Let. 1, 437-441.
681 Sahebi, S., Sheikhi, M., Ramavandi, B., 2019. A new biomimetic aquaporin thin film composite
682 membrane for forward osmosis: Characterization and performance assessment. Desalin.
683 Water Treat. 148, 42-50.
684 Sauchelli, M., Pellegrino, G., D'Haese, A., Rodriguez-Roda, I., Gernjak, W., 2018. Transport of
685 trace organic compounds through novel forward osmosis membranes: Role of membrane
686 properties and the draw solution. Water Res. 141, 65-73.
687 Shaffer, D.L., Werber, J.R., Jaramillo, H., Lin, S., Elimelech, M., 2015. Forward osmosis: Where
688 are we now? Desalination 356, 271-284.
689 Shaffer, D.L., Yip, N.Y., Gilron, J., Elimelech, M., 2012. Seawater desalination for agriculture by
690 integrated forward and reverse osmosis: Improved product water quality for potentially
691 less energy. J. Membrane Sci. 415, 1-8.
692 Stewart, J., 2016. Mopac2016, Stewart Computational Chemistry, Colorado Springs, CO.
693 U.S. EPA, 2001. User's guide for water9 software, US Environmental Protection Agency, Office
694 of Air Quality Planning and Standards.

695 U.S. EPA, 2010. National primary drinking water regulations, U.S. Government Printing Office,
696 Washington, DC.
697 Vaes, W.H.J., Urrestarazu Ramos, E., Verhaar, H.J.M., Cramer, C.J., Hermens, J.L.M., 1998.
698 Understanding and estimating membrane/water partition coefficients: Approaches to
699 derive quantitative structure property relationships. Chem. Res. Toxicol. 11, 847-854.
700 Van Oss, C.J., 2006. Interfacial forces in aqueous media, CRC press.
701 Van Oss, C.J., 2007. Development and applications of the interfacial tension between water and
702 organic or biological surfaces. Colloid. Surface. B 54, 2-9.
703 Wagner, E.D., Plewa, M.J., 2017. Cho cell cytotoxicity and genotoxicity analyses of disinfection
704 by-products: An updated review. J. Environ. Sci.-China 58, 64-76.
705 Wang, J., Mo, Y., Mahendra, S., Hoek, E.M.V., 2014. Effects of water chemistry on structure and
706 performance of polyamide composite membranes. J. Membrane Sci. 452, 415-425.
707 Xia, L., Andersen, M.F., Hélix-Nielsen, C., McCutcheon, J.R., 2017. Novel commercial aquaporin
708 flat-sheet membrane for forward osmosis. Ind. Eng. Chem. Res. 56, 11919-11925.
709 Xiang, X., Zou, S., He, Z., 2017. Energy consumption of water recovery from wastewater in a
710 submerged forward osmosis system using commercial liquid fertilizer as a draw solute.
711 Sep. Purif. Technol. 174, 432-438.
712 Xie, M., Luo, W.H., Guo, H., Nghiem, L.D., Tang, C.Y., Gray, S.R., 2018. Trace organic
713 contaminant rejection by aquaporin forward osmosis membrane: Transport mechanisms
714 and membrane stability. Water Res. 132, 90-98.
715 Xie, M., Nghiem, L.D., Price, W.E., Elimelech, M., 2012. Comparison of the removal of
716 hydrophobic trace organic contaminants by forward osmosis and reverse osmosis. Water
717 Res. 46, 2683-2692.

718 Xie, M., Nghiem, L.D., Price, W.E., Elimelech, M., 2014. Relating rejection of trace organic
719 contaminants to membrane properties in forward osmosis: Measurements, modelling and
720 implications. Water Res. 49, 265-274.
721 Xu, J., Kralles, Z.T., Hart, C.H., Dai, N., 2020. Effects of sunlight on the formation potential of
722 dichloroacetonitrile and bromochloroacetonitrile from wastewater effluents. Environ. Sci.
723 Technol. 54, 3245-3255.
724 Xu, J., Tran, T.N., Lin, H., Dai, N., 2018. Removal of disinfection byproducts in forward osmosis
725 for wastewater recycling. J. Membrane Sci. 564, 352-360.
726 Yangali-Quintanilla, V., Li, Z.Y., Valladares, R., Li, Q.Y., Amy, G., 2011. Indirect desalination
727 of red sea water with forward osmosis and low pressure reverse osmosis for water reuse.
728 Desalination 280, 160-166.
729 Yuan, H., Abu-Reesh, I.M., He, Z., 2015. Enhancing desalination and wastewater treatment by
730 coupling microbial desalination cells with forward osmosis. Chem. Eng. J. 270, 437-443.
731 Zeng, T., Plewa, M.J., Mitch, W.A., 2016. N-nitrosamines and halogenated disinfection
732 byproducts in u.S. Full advanced treatment trains for potable reuse. Water Res. 101, 176-
733 186.
734 Zheng, L., Price, W.E., McDonald, J., Khan, S.J., Fujioka, T., Nghiem, L.D., 2019. New insights
735 into the relationship between draw solution chemistry and trace organic rejection by
736 forward osmosis. J. Membrane Sci. 587, 117184.
737 Zou, S., He, Z., 2016. Enhancing wastewater reuse by forward osmosis with self-diluted
738 commercial fertilizers as draw solutes. Water Res. 99, 235-243.
739 Zou, S., Qin, M., He, Z., 2019. Tackle reverse solute flux in forward osmosis towards sustainable
740 water recovery: Reduction and perspectives. Water Res. 149, 362-374.

741 Zou, S., Yuan, H., Childress, A., He, Z., 2016. Energy consumption by recirculation: A missing
742 parameter when evaluating forward osmosis. Environ. Sci. Technol. 50, 6827-6829.

743 **Figure 1.** Linear regression of Log ($K^{MSL}_{DBP,Salt}/K^{MSL}_{DBP,DI}$) as a function of NaCl concentration C^S (M).

744 The slope of the curve is the Setschenow constant (k^{Salt}_{DBP}, M^{-1}). Abbreviations of DBPs are shown

745 in Table S2.

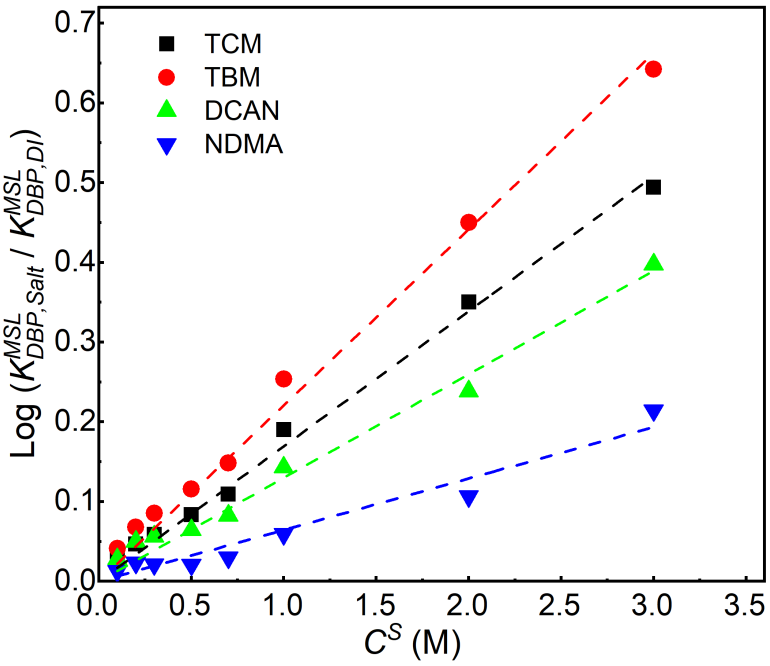

746

Figure 2. DBP rejection by Aquaporin membrane using (a) varying draw solute species and (b) varying NaCl concentrations. *R* = stabilized rejection. The water fluxes of the experiments are shown in Table S4. Initial concentrations of nitrosamines and halogenated DBPs in the feed were 10 and 20 μg·L^{-1}, respectively. Feed solution pH was 6.5-7.5 unbuffered. Room temperature at 20 °C. The rejection values are shown in Table S6. Abbreviations: THM, trihalomethane; HAN, haloacetonitrile; HK, haloketone. Abbreviation of individual DBP is shown in Table S2.

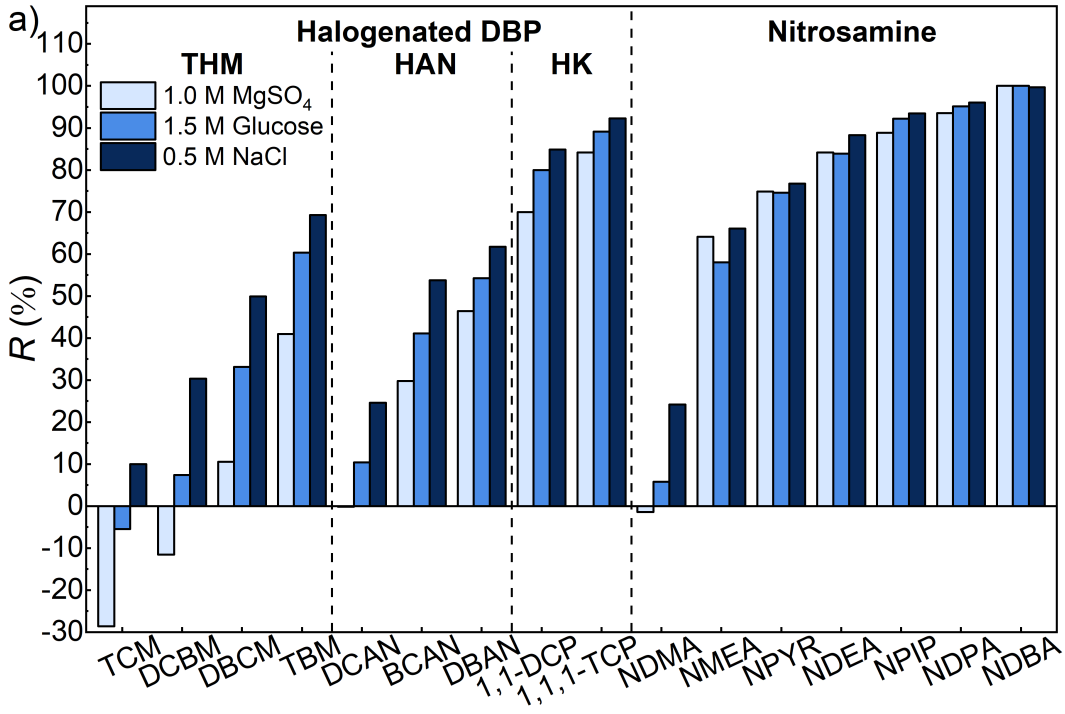

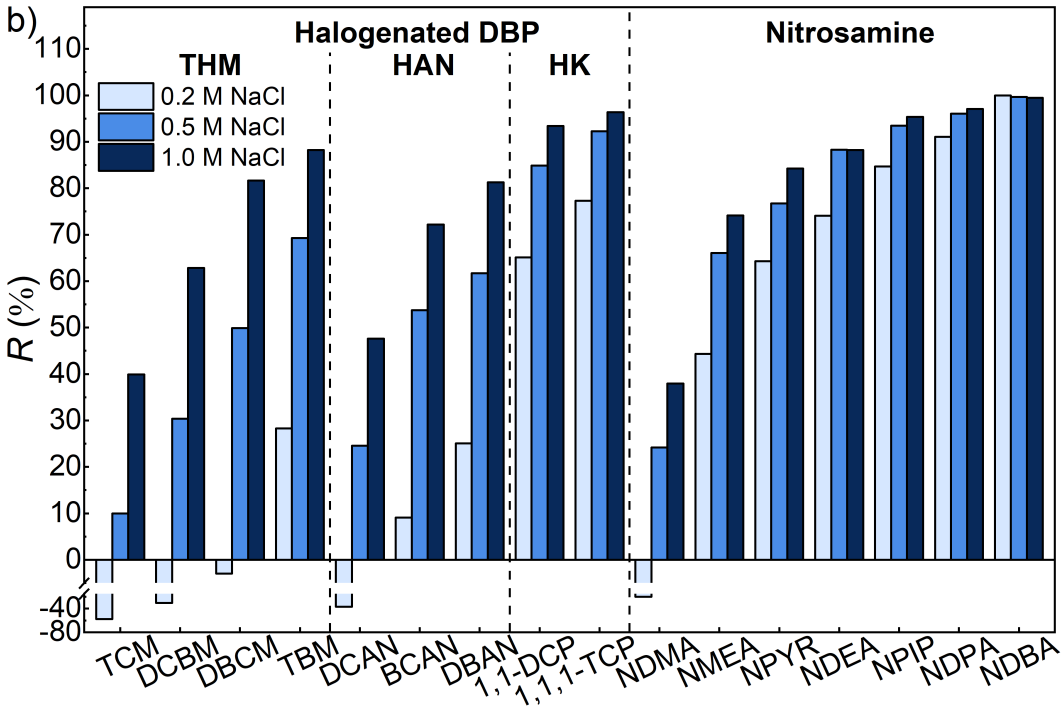
b)
Halogenated DBP
Nitrosamine
THM
HAN
HK
0.2 M NaCl
0.5 M NaCl
1.0 M NaCl
R (%)
110
100
90
80
70
60
50
40
30
20
10
0
-40
-80
TCM
DCBM
DBCM
TBM
DCAN
BCAN
DBAN
1,1-DCP
1,1,1-TCP
NDMA
NMEA
NPYR
NDEA
NPIP
NDPA
NDBA

754

Figure 3. Relationship between DBP permeance in bench-scale FO experiments and reverse salt flux for (a) trihalomethanes, (b) haloacetonitriles and haloketones, and (c) nitrosamines. Draw solute was introduced in the legend. The reverse salt flux and water flux of the experiments are shown in Table S4. The DBP permeance values are shown in Table S7. Abbreviations of DBPs are shown in Table S2.

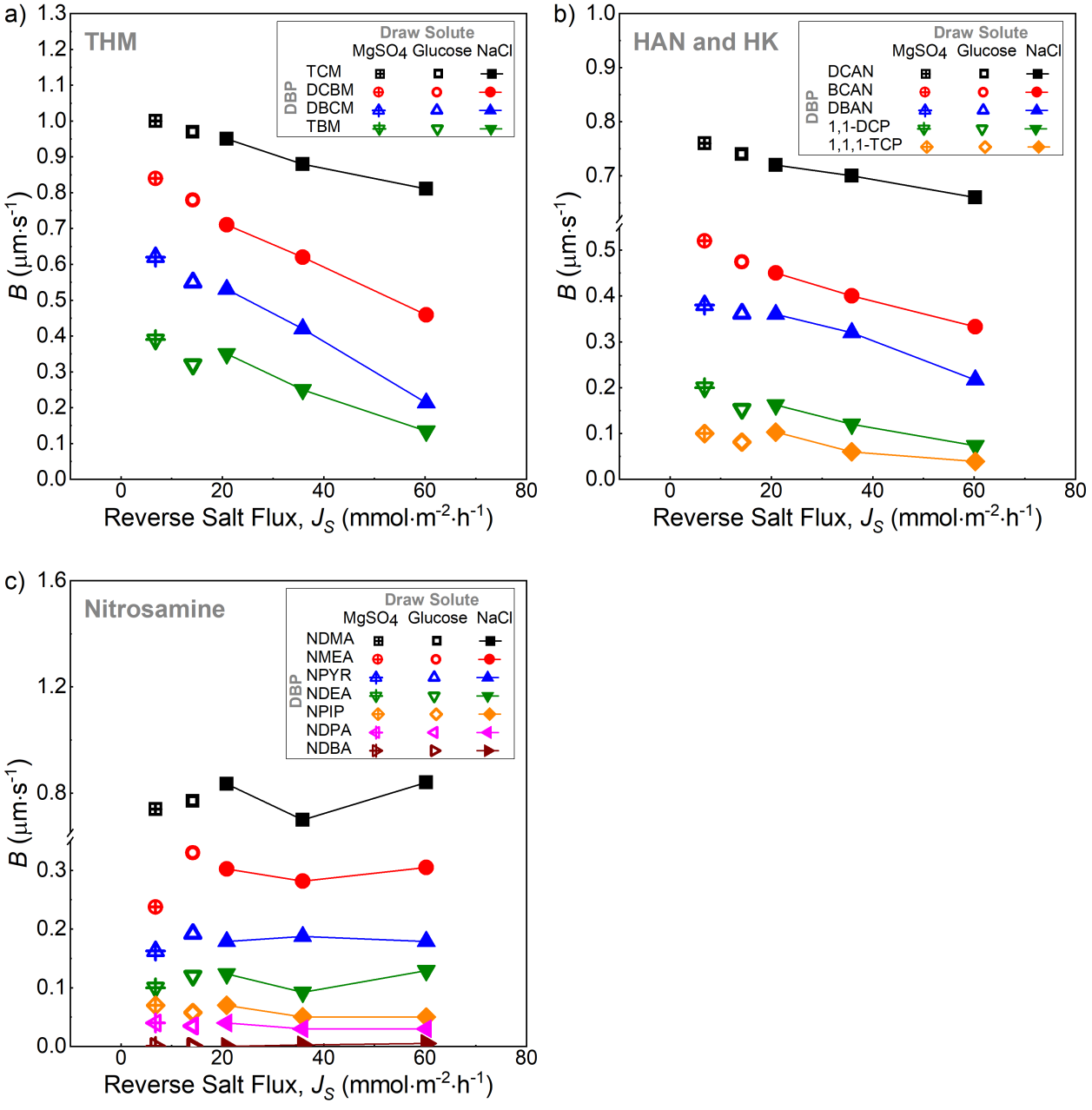

Figure 4. Permeance of halogenated DBPs in the diffusion cell test. Details of the experimental protocol are shown in section 2.3. The initial concentrations of DBPs in the feed and the draw sides were 2 mg·L^{-1} and 50 μg·L^{-1}, respectively. The DBP permeance values are shown in Table S8. Error bars represent the range from duplicate experiments.

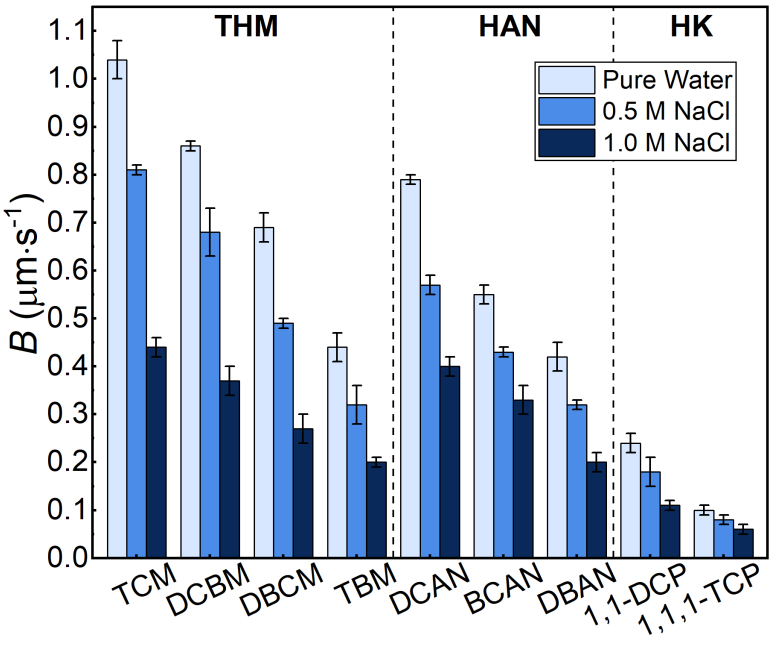

Figure 5. Relationship between the change in DBP permeance in the presence of draw solutes with respect to the molecular volume of DBPs. DBP permeance determined in FO experiments using (a) 1.0 M $MgSO_4$, (b) 1.5 M glucose, or (c) 1.0 M NaCl as the draw solution was normalized by the DBP permeance determined in diffusion cell experiments with pure water. Pearson's (linear) and Spearman's (monotonic) correlation tests were performed, and the significance level α was set at 0.05. The molecular volume of DBPs is shown in Table S2.

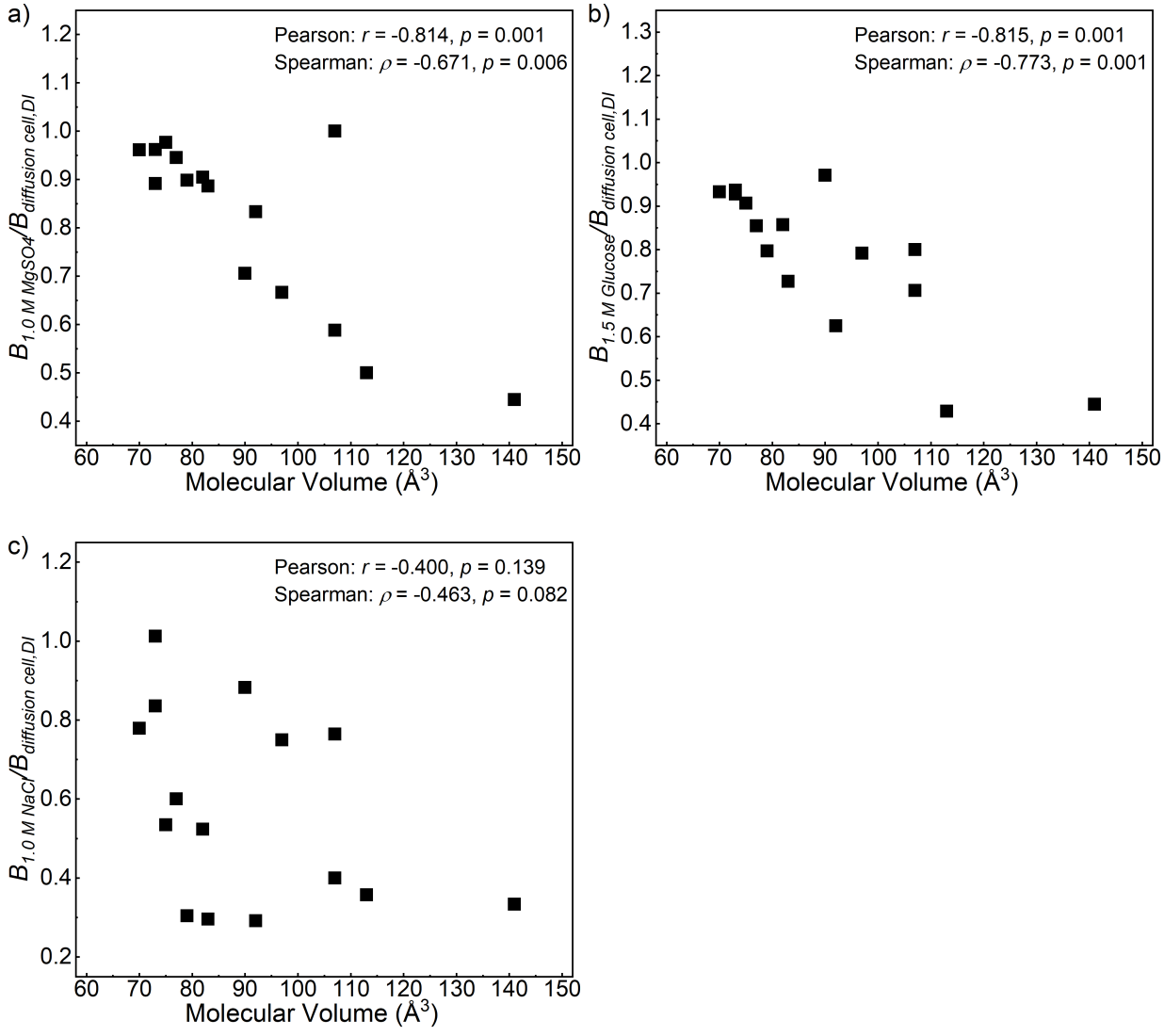

Figure 6. Relationship between the change in DBP permeance in the presence of draw solutes with respect to the Log K_{ow} of DBPs. DBP permeance determined in FO experiments using (a) 1.0 M $MgSO_4$, (b) 1.5 M glucose, or (c) 1.0 M NaCl as the draw solution was normalized by the DBP permeance determined in diffusion cell experiments with pure water. Pearson's (linear) and Spearman's (monotonic) correlation tests were performed, and the significance level α was set at 0.05. The Log K_{ow} values of DBPs are shown in Table S2.

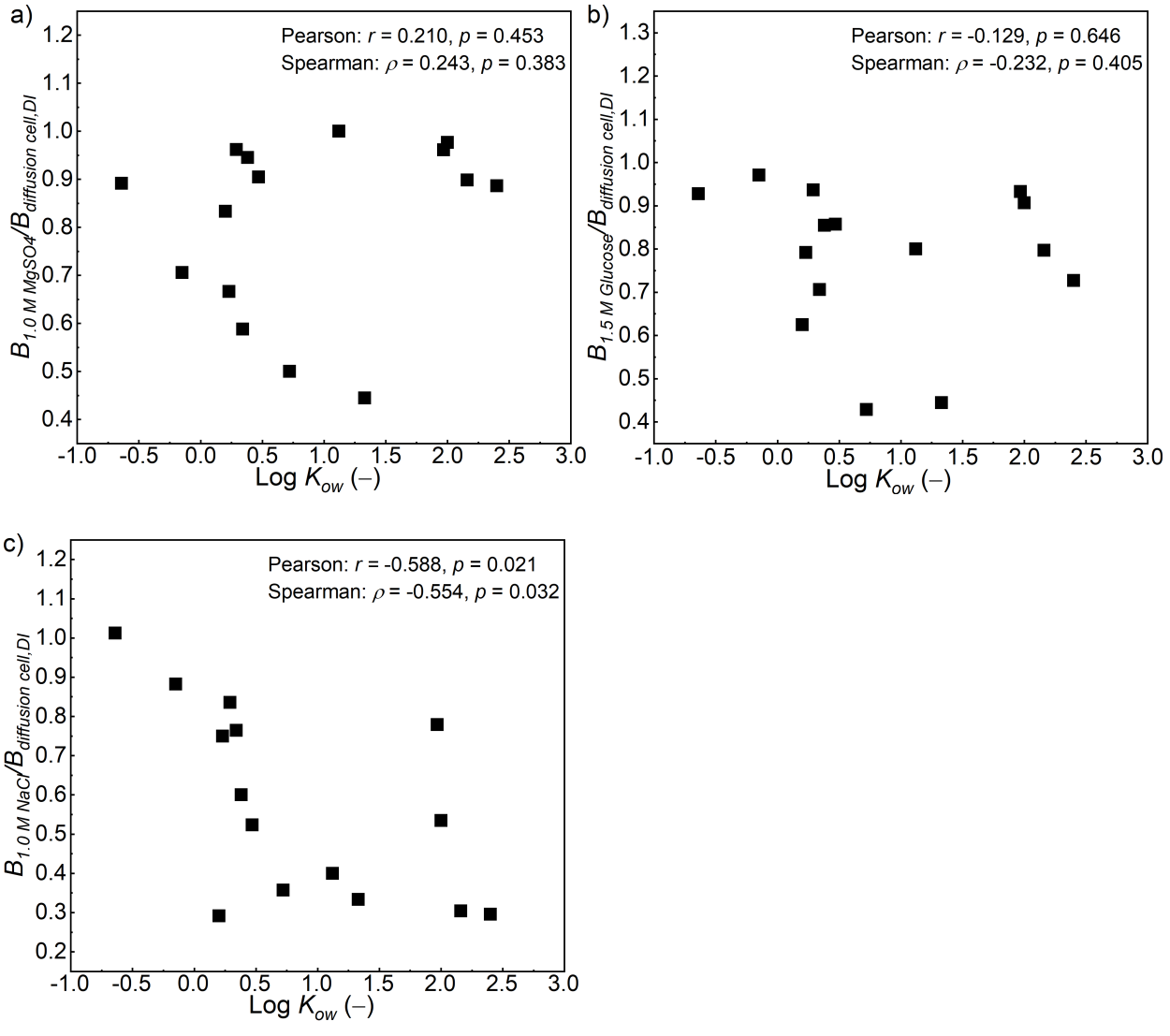

783 **Figure 7.** The ratio of B_{AL}^{S} to B_{AL}^{DI} as a function of NaCl concentration in the draw solution.

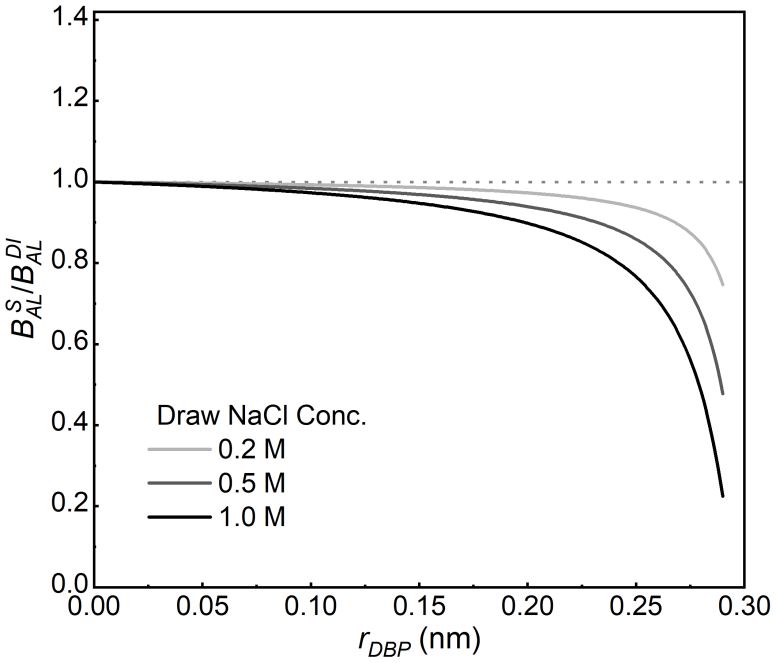

784

Figure 8. Comparison of (a–b) DBP permeance and (c–d) DBP rejection determined in bench-scale FO experiments with those predicted by the conventional solution-diffusion (SD) model or the modified SD (M-SD) model. Initial NaCl concentrations in draw reservoir were (a, c) 0.2 M and (b, d) 1.0 M. DBP permeance values are shown in Tables S7 and S11, and DBP rejection values are shown in Tables S6 and S12. Abbreviations of DBPs are shown in Table S2.

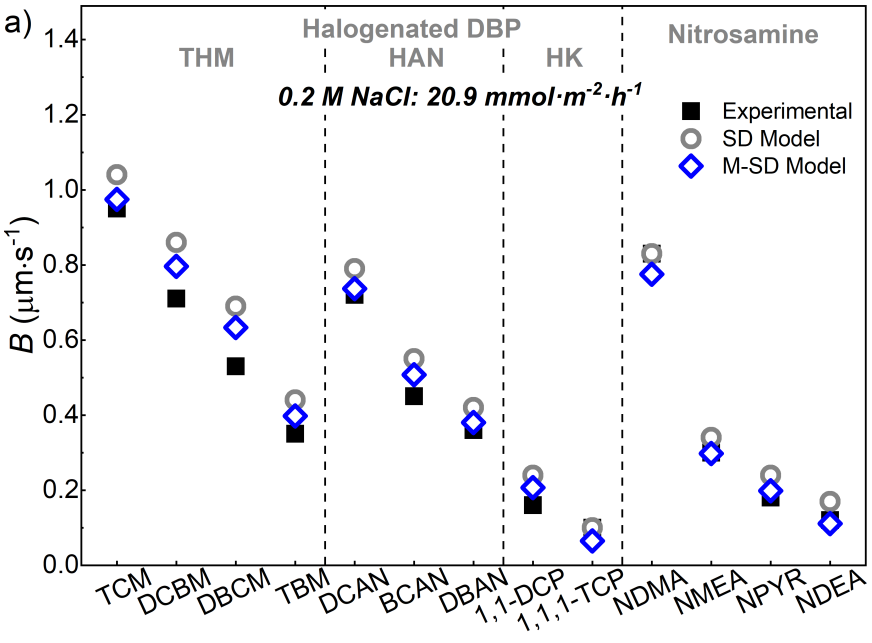

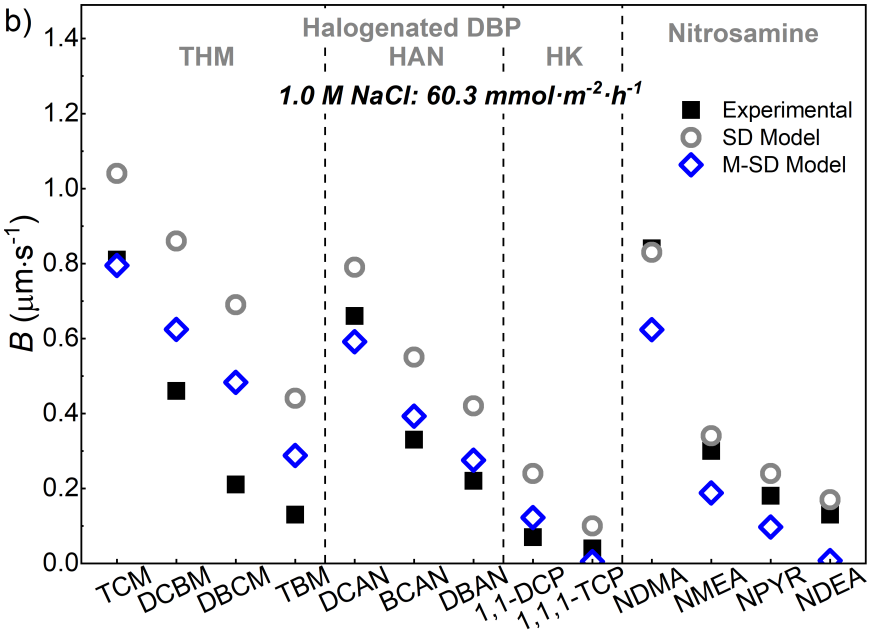

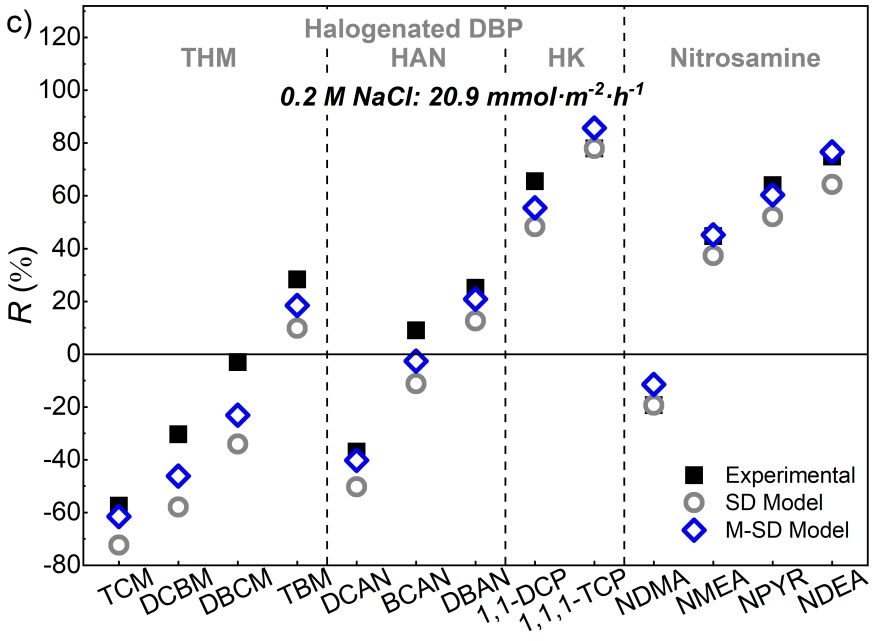
c)
Halogenated DBP
THM
HAN
HK
Nitrosamine
0.2 M NaCl: 20.9 mmol·m-2·h-1
R (%)
120
100
80
60
40
20
0
-20
-40
-60
-80
Experimental
SD Model
M-SD Model
TCM
DCBM
DBCM
TBM
DCAN
BCAN
DBAN
1,1-DCP
1,1,1-TCP
NDMA
NMEA
NPYR
NDEA

792

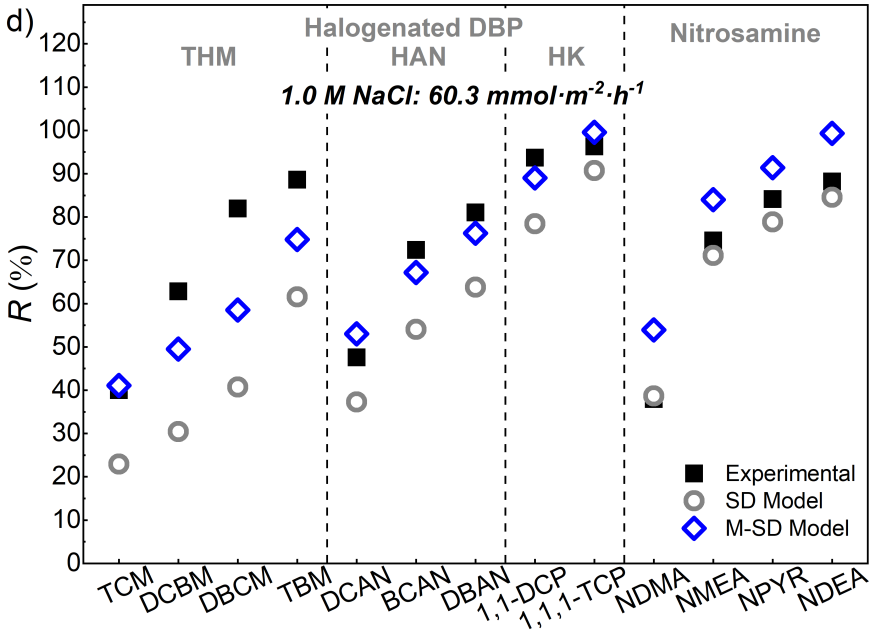
d)
Halogenated DBP
THM
HAN
HK
Nitrosamine
1.0 M NaCl: 60.3 mmol·m-2·h-1
R (%)
120
110
100
90
80
70
60
50
40
30
20
10
0
Experimental
SD Model
M-SD Model
TCM
DCBM
DBCM
TBM
DCAN
BCAN
DBAN
1,1-DCP
1,1,1-TCP
NDMA
NMEA
NPYR
NDEA

793

Figure 9. Comparison of the contribution of steric hindrance and retarded diffusion in the M-SD model. The DBP permeance determined from experiments and models is shown in Tables S7 and S11, respectively. Abbreviations of DBPs are shown in Table S2.

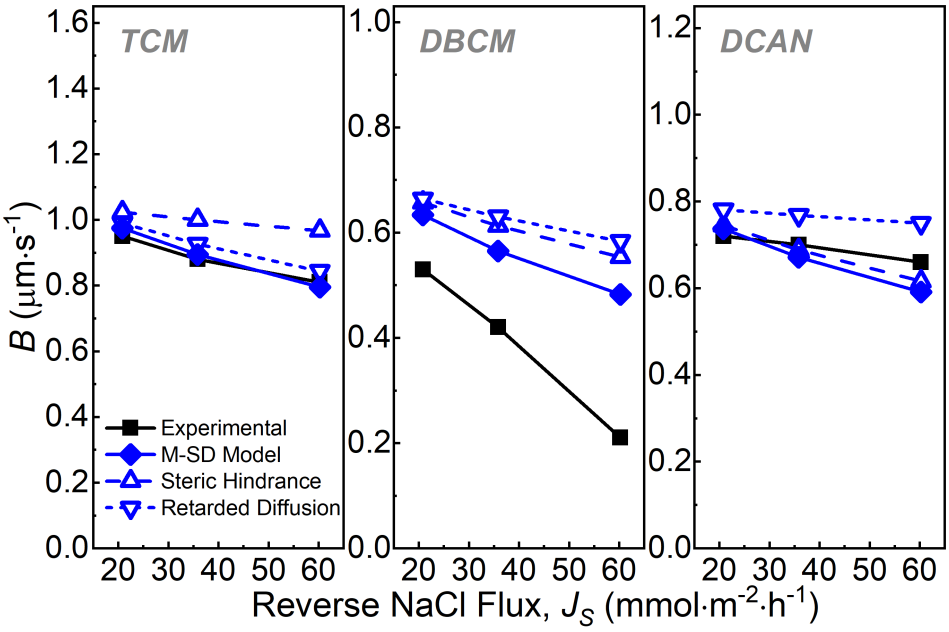

Table 1. Surface tension components of the support layer of Aquaporin membrane and DBPs tested in this study.

Membrane or DBPs		Surface Tension Components ($mJ \cdot m^{-2}$)		
		γ^{LW}	γ^{+}	γ^{-}
Aquaporin Membrane	Support Layer[a]	43.7	0.0	24.4
DBP	TCM[b]	27.2	1.5	0.0
	TBM[c]	41.5	1.7	0.0
	DCAN[a]	61.2	0.0	20.8
	NDMA[a]	36.5	0.0	32.6

[a]Determined in this study.

[b](Van Oss 2006).

[c](Janczuk et al. 1993).

798

Table 2. Partitioning coefficients of DBPs between the membrane support layer and Milli-Q water as well as Setschenow constants of DBPs.

DBPs	Partitioning Coefficient, $K_{DBP,DI}^{MSL}$ (–)		Setschenow Constant, k_{DBP}^{Salt} (M^{-1})	
	Contact Angle Method[a]	Regression Model Method[b]	Contact Angle Method[a]	Regression Model Method[b]
TCM	3.926	3.369	0.170	0.193
DCBM		3.640		0.194
DBCM	–	3.711	–	0.200
TBM	5.296	4.249	0.221	0.210
DCAN	1.612	1.711	0.130	0.126
BCAN		1.978		0.129
DBAN		2.034		0.133
1,1-DCP	–	2.176	–	0.122
1,1,1-TCP		3.287		0.159
NDMA	0.992	1.221	0.065	0.088
NMEA		2.023		0.108
NPYR	–	2.572	–	0.123
NDEA		2.461		0.128

[a]Calculated using surface tension components as described in section 3.2.2.

[b]Estimated based on equations 18 and 19 for $K_{DBP,DI}^{MSL}$ and k_{DBP}^{Salt}, respectively.

799

Table 3. Effective pore radius of the active layer (r_p^S, nm) and DBP permeance through the active layer when different NaCl solutions were used as the draw solution (B_{AL}^S, μm·s^{-1}).

Test Mode	Initial NaCl Concentration in the Draw Reservoir, C_D^S (M)	Reverse NaCl Flux, J_S (mmol·m^{-2}·h^{-1})	Effective Pore Radius, r_p^S (nm)	DBP Permeance through Active Layer, B_{AL}^S (μm·s^{-1})			
				TCM	TBM	DCAN	NDMA
Diffusion Cell	0	0	0.305	4.96	0.81	1.13	1.06
FO	0.2	20.9	0.303	4.60	0.73	1.04	0.97
	0.5	35.8	0.300	4.17	0.62	0.93	0.87
	1.0	60.3	0.297	3.65	0.50	0.80	0.75

800

Table 4. Retardation factor of the support layer for each DBP (R_r, dimensionless).

DBPs	Retardation Factor, R_r (–)							
	Contact Angle Method[a]				Regression Model Method[a]			
	0 M[b] (0)[d]	0.2 M[c] (20.9)	0.5 M[c] (35.8)	1.0 M[c] (60.3)	0 M[b] (0)	0.2 M[c] (20.9)	0.5 M[c] (35.8)	1.0 M[c] (60.3)
TCM	4.576	4.870	5.285	5.923	4.019	4.306	4.717	5.360
DCBM					4.290	4.603	5.049	5.747
DBCM			–		4.361	4.690	5.161	5.901
TBM	5.946	6.467	7.221	8.423	4.899	5.295	5.866	6.768
DCAN	2.262	2.354	2.480	2.670	2.361	2.455	2.585	2.779
BCAN					2.628	2.739	2.893	3.125
DBAN					2.684	2.802	2.966	3.212
1,1-DCP			–		2.826	2.942	3.101	3.339
1,1,1-TCP					3.937	4.167	4.489	4.982
NDMA	1.642	1.670	1.707	1.760	1.871	1.918	1.981	2.072
NMEA					2.673	2.768	2.898	3.090
NPYR			–		3.222	3.360	3.550	3.834
NDEA					3.111	3.248	3.439	3.723

[a]Calculated using $K_{DBP,DI}^{MSL}$ and k_{DBP}^{Salt} determined in section 3.2 of the main text.

[b]Diffusion cell test using Milli-Q water.

[c]Initial NaCl concentration of draw reservoir in FO test.

[d]The value in the parenthesis is the reverse NaCl flux with the unit of $mmol \cdot m^{-2} \cdot h^{-1}$.

801